Synthesis and molecular docking study of α-aminophosphonates as potential multi-targeting antibacterial agents

Rana Neiber, Nadia Samak, Jianmin Xing, Elshaymaa Elmongy, Ahmed Galhoum, Ibrahim El-Tantawy El Sayed, Eric Guibal, Jiayu Xin, Xingmei Lu

▶ **To cite this version:**

Rana Neiber, Nadia Samak, Jianmin Xing, Elshaymaa Elmongy, Ahmed Galhoum, et al.. Synthesis and molecular docking study of α-aminophosphonates as potential multi-targeting antibacterial agents. Journal of Hazardous Materials, 2024, 465, pp.133203. 10.1016/j.jhazmat.2023.133203 . hal-04402213

HAL Id: hal-04402213

https://imt-mines-ales.hal.science/hal-04402213

Submitted on 27 Mar 2024

HAL is a multi-disciplinary open access archive for the deposit and dissemination of scientific research documents, whether they are published or not. The documents may come from teaching and research institutions in France or abroad, or from public or private research centers.

L'archive ouverte pluridisciplinaire **HAL**, est destinée au dépôt et à la diffusion de documents scientifiques de niveau recherche, publiés ou non, émanant des établissements d'enseignement et de recherche français ou étrangers, des laboratoires publics ou privés.

Synthesis and molecular docking study of α-aminophosphonates as potential multi-targeting antibacterial agents

Rana R. Neiber [a,b,c], Nadia A. Samak [b,d,e,*], Jianmin Xing [b,d], Elshaymaa I. Elmongy [f], Ahmed A. Galhoum [g,**], Ibrahim El-Tantawy El Sayed [h,**], Eric Guibal [i], Jiayu Xin [a,c,j], Xingmei Lu [a,c,j,k,***]

[a] Beijing Key Laboratory of Ionic Liquids Clean Process, CAS Key Laboratory of Green Process and Engineering, Institute of Process Engineering, Chinese Academy of Sciences, 100190 Beijing, China

[b] College of Chemical Engineering, University of Chinese Academy of Sciences, 19 A Yuquan Road, 100049 Beijing, China

[c] School of Chemistry and Chemical Engineering, University of Chinese Academy of Sciences, 100049 Beijing, China

[d] CAS Key Laboratory of Green Process and Engineering & State Key Laboratory of Biochemical Engineering, Institute of Process Engineering, Chinese Academy of Sciences, Beijing 100190, China

[e] Aquatic microbiology department, Faculty of Chemistry, University of Duisburg-Essen, 45141 Essen, Germany

[f] Department of Pharmaceutical Sciences, College of Pharmacy, Princess Nourah bint Abdulrahman University, P.O. BOX 84428, Riyadh 11671, Saudi Arabia

[g] Nuclear Materials Authority, P.O. Box 530, El-Maadi, Cairo, Egypt

[h] Chemistry Department, Faculty of Science, Menoufia University, Shebin El-Kom, Egypt

[i] Institut Mines Telecom–Mines Alès, C2MA, 6 avenue de Clavières, F-30319 Alès cedex, France

[j] Innovation Academy for Green Manufacture, Chinese Academy of Sciences, Beijing 100190, China

[k] Department of Chemistry, University of Chinese Academy of Sciences, 100049 Beijing, China

HIGHLIGHTS

- α-aminophosphonates were synthesized and their antibacterial activity was tested.
- Minimum inhibitory concentration values reached in the range of 3.13–6.25 μg/mL.
- Compound [B] showed efficient eradication of extracellular polymeric substances.
- Molecular docking revealed that compounds [B] bind strongly to protein structures.
- α-Amp$_s$ moiety is promising to develop new antibacterial and anti-biofilm agents.

GRAPHICAL ABSTRACT

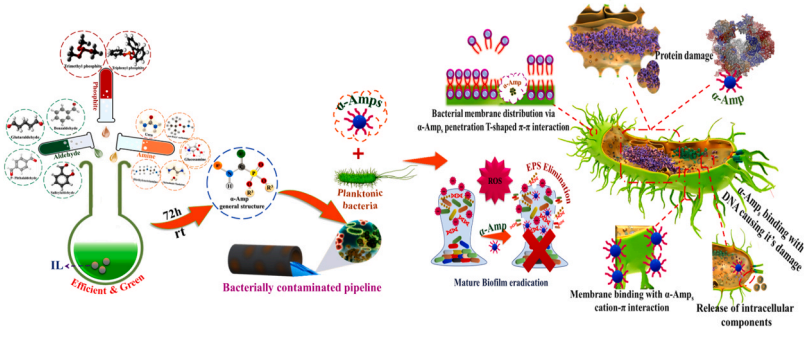

* Corresponding author at: CAS Key Laboratory of Green Process and Engineering & State Key Laboratory of Biochemical Engineering, Institute of Process Engineering, Chinese Academy of Sciences, Beijing 100190, China

** Corresponding authors.

*** Corresponding author at: Beijing Key Laboratory of Ionic Liquids Clean Process, CAS Key Laboratory of Green Process and Engineering, Institute of Process Engineering, Chinese Academy of Sciences, 100190 Beijing, China.

E-mail addresses: nadia@ipe.ac.cn (N.A. Samak), galhoum_nma@yahoo.com (A.A. Galhoum), ibrahimtantawy@yahoo.co.uk (I.E.-T. El Sayed), xmlu@ipe.ac.cn (X. Lu).

Keywords:
Aminophosphonates
Bacteria
Docking study
Anti-bacterial
Anti-biofilm

A B S T R A C T

Antibacterial compounds that reduce extracellular polymeric substances (EPS) are needed to avoid bacterial biofilms in water pipelines. Herein, green one-pot synthesis of α-aminophosphonates (α-Amp_s) [A-G] was achieved by using ionic liquid (IL) as a Lewis acid catalyst. The synthesized α-Amp analogues were tested against different bacteria such as *Bacillus subtilis*, *Escherichia coli*, and *Pseudomonas aeruginosa*. The representative [B] analogue showed an efficient antibacterial effect with MIC values of 3.13 μg/mL for *E. coli*, *P. aeruginosa,* and 6.25 μg/mL for *B. subtilis*. Additionally, a strong ability to eliminate the mature bacterial biofilm, with super-MIC values of 12.5 μg/mL for *E. coli*, *P. aeruginosa*, and 25 μg/mL for *B. subtilis*. Moreover, bacterial cell disruption by ROS formation was also tested, and the compound [B] revealed the highest ROS level compared to other compounds and the control, and efficiently destroyed the extracellular polymeric substances (EPS). The docking study confirmed strong interactions between [B] analogue and protein structures with a binding affinity of −6.65 kCal/mol for the lyase protein of gram-positive bacteria and −6.46 kCal/mol for DNA gyrase of gram-negative bacteria. The results showed that α-Amp_s moiety is a promising candidate for developing novel antibacterial and anti-biofilm agents for clean water supply.

1. Introduction

Pathogenic biofilms are a significant healthcare issue due to their ability to exert antibiotic resistance leading to the severity of critical illness and even death. Many efforts have been made so far to target bacteria in biofilms, but a comprehensive antibacterial effect has not yet been attained. [16,4,7]. A biofilm refers to a stratified community of bacteria that develops within a matrix, commonly known as a slime layer, on surfaces that come into contact with water. The existence of these organisms within the infrastructure of water pipe networks can rise to a diverse array of issues pertaining to both water quality and operational efficiency [14,41,57]. Furthermore, the presence of biofilm has the potential to impact the sensory properties of water, including taste and odor. Additionally, when biofilms form on surfaces composed of ferrous metals, they can lead to corrosion of the pipes and subsequent release iron particles into the water. Reduction in the permeation of bacterial cell membrane, alteration in bacterial cell physiology, and a rise in proton-dependent active efflux are the current routes to cause antibiotic drug resistance (ADR). The release of antibiotic-modifying enzymes by bacteria [60] and the irrational use of antibacterial agents, especially in developing countries, have led to an increase in the drug resistance of such microorganisms. Among the many causes, inappropriate drug practices, poor patient education, lack of proper diagnostics, and illicit use of antibiotics, followed by ineffective medications, are the primary routes contributing to ADR [5].

Bacterial biofilms are a slime matrix produced by different species of bacteria, which are surrounded by extra polymeric substances (EPS) [10, 38,69]. This matrix provides protection from the detrimental impacts of biocides, detergents, and antibiotics. Bacterial biofilms have the ability to proliferate inside various aquatic environments, including water pipelines and swimming pools [29]. The adverse impact of bacterial biofilms has prompted the scientific community to develop novel materials that possess improved antimicrobial and antibiofilm characteristics. Common bacterial strains present in bacterial biofilms in water sources include *E. coli*, *P. aeruginosa,* and *B. subtilis* [13,27,37]. *E. coli* and *P. aeruginosa* is a Gram-negative bacterium, which is a significant cause of meningitis, septicemia, urinary tract, intestinal infections, and acute infections, such as ventilator-associated pneumonia (VAP) [29]. *B. subtilis* is Gram-positive type bacteria, which widely spreads in surface water, and it is known to be associated with bacteremia, endocarditis, pneumonia, and septicemia [45,58,61]. Here, eliminating bacterial biofilms is challenging owing to the intricacy of their chemical composition and physical structure. Basically, the formation of microbial biofilms involves the following steps: (a) the microbial cells accommodate over the wet external surface; (b) cell growth and extracellular polymeric substances are shaped; (c) and the biofilm gets strengthened via bacterial activities and growth. Thus, effective antibacterial compounds that may be disseminated in water sources or incorporated into coating materials to limit microbial growth and biofilms in water pipelines are needed urgently.

The inherent antibiotic resistance of such biofilms necessitates the rapid development of effective new anti-biofilm agents [8]. Substances such as α-aminophosphonates, as alternatives to α-amino acids, play a significant role in agricultural, medical [23], and environmental fields [26,55]. Recent research for the development of antibacterial drugs highlighted the promising features of antibiofilm formation and high efficiency. Hence, α-aminophosphonates demonstrated remarkable antibacterial efficacy and superb biocompatibility. The promising properties of α-aminophosphonates have recently retained great attention for developing antibacterial drugs [17,63]. Based on, providing a biocompatible layer on water facilities may be a solution for preventing the growth of microorganism or the formation of biofilm. Additionally, the chemical structure of phosphide compounds may promote electrostatic exchanges with bacteria's surface charge species, forming phospholipid membranes that hinder membrane-water interactions. For distinctive attributes of this compound, it may be employed in a dispersed form for the remediation of contaminated water pipelines. Subsequently, these pipelines can undergo multiple washes to eliminate α-aminophosphonates. On the other hand, it can be incorporated into the surface of reverse osmosis (RO) membranes, which are commonly utilized for water filtration purposes. Aminophosphonate-based materials with various functionalities have already been described, including the grafting of reactive moieties onto titanium oxide, zirconium, and apatite [39,53]. Wastewater treatment has also been done using commercial resins containing α-aminophosphonate groups [33]. However, the duration and cost of the process are undoubtedly increased by the two-step synthesis of these composite adsorbents. In this context, one-pot synthesis of α-aminophosphonate derivatives and their application as antibacterial agents Thus, the selection of α-aminophosphonates might be an effective strategy to build processes having the potential to combat drug-resistant bacteria infection owing to their potent antibacterial activity and ability to restrain the growth of microorganism or biofilm formation.

Herein, a series of α-aminophosphonates (α-Amp_s) are synthesized using a metal-free green catalyst, and their antibacterial efficiency and antibiofilm activity are evaluated. Our earlier research has demonstrated the significance of the environment of phosphonate group on their reactivity in wastewater treatment. To further understand these effects and make α-aminophosphonate-based comparable antibacterial treatments more effective, this research is expanded to include other alterations of this environment. The inductive effect of substituents, and hydrophilic behavior, can all be used to influence microbial growth. This particular addition offers supplemental data on the impact of various analogs of α-aminophosphonate-based antibacterial compounds on ROS production, membrane disruption, and EPS component decrease. Another ground-breaking innovation is the straightforward and safe

alternative technique, which uses ionic liquid as a safe catalyst rather than a harmful one. Linked to the in-depth characterization of materials, those conjunctions of studies contribute to a complete and innovative approach. The one-pot synthesis of α-aminophosphonates (α-Amp$_s$) is carried out at ambient temperature for 72 h; the ionic liquid (IL) acts as a Lewis acid catalyst. Seven different analogues of α-Amp were prepared by altering the type of aldehyde, amine, and phosphite groups (respectively named [A-G]). One of the major contributions of this work will consist of evaluating the effect of the different α-Amp$_s$ analogues on antibacterial inhibition. The structure and chemical functionality of α-Amp$_s$ were verified utilizing FT-IR and NMR spectroscopy, also were tested to evaluate their antibacterial activity against the bacterial strains of *E. coli*, *P. aeruginosa*, and *B. subtilis*. The minimum inhibitory concentration (MIC) values were determined. The representative [B] analogue realized superior efficiency against the bacterial strains of each tested bacteria compared to its other competitive derivatives. Confocal microscopy and Scanning Electron Microscopy (SEM) are also utilized to evaluate the biological state of the biofilms (and the destruction of their extracellular polymeric layer, which contains protein, nucleic acid, and polysaccharides). The inhibition of bacterial biofilms was further analyzed through live and dead cells study using Syto9 and propidium iodine stain, respectively. In addition, molecular docking further confirmed that compound [B] binds strongly to protein structures. The present study would play a vital role in understanding the easy preparation of α-Amp compounds and how specific functional groups could significantly affect the antibacterial activity. This may be of critical importance for designing antibacterial biofilm material, particularly for cleaning water pipelines for domestic consumption, and might play a crucial role in reaching clean-water goals in under-developing nations.

2. Materials and methods

2.1. Materials

Various chemicals were used to synthesize α-Amp analogues. The details of the chemicals and bacteria supplier unit were given in the supplementary information (**Section S1**).

2.2. Synthesis of α-aminophosphonate analogues

A simple one-pot reaction was carried out to prepare the α-Amp analogues with a simple general reaction as displayed in Scheme S1. In brief, amine (mono or bis: *tert*-butyl carbamate, glucosamine, urea, ethylenediamine monohydrate, and diethylenetriamine) were condensed with an aldehyde (mono or di: benzaldehyde, salicylaldehyde, glutaraldehyde, and p-phthalaldehyde), and phosphite (trimethyl phosphite, and triphenyl phosphite) using different ratios. The reaction was set for 72 h at the ambient condition in a Lewis acid catalyst (20% mmol ionic liquid) that facilitated green synthesis conditions (dissolved in acetonitrile solvent). Thin-layer chromatography was used for the confirmation (TLC) with a mobile phase composition of dichloromethane and hexane (1:3). In the end, deionized water and methanol were used to wash the mixture, and the solid residue was filtered out and dried in a 60 °C oven.

Different techniques were used to characterize α-Amp analogues for their structural confirmation. The details of the techniques were provided in supplementary information (**Section S2**).

2.3. Antibacterial activity

2.3.1. Modified Kirby-Bauer antibacterial susceptibility test

A modified Kirby-Bauer agar well diffusion technique was used to evaluate the antibacterial performance and activity of α-Amp analogues against the target bacteria. In a typical experiment, the sterile and hardened Mueller-Hinton agar plates were inoculated with 7.5×10^4 CFU/mL bacterial culture suspension followed by incubation of Petri plates for 15 min to permit the culture to absorb into the medium. Next, all the Petri plates were drilled with 4 wells (6 mm) using a cork borer to inject and hold synthetic α-Amp compounds (dissolved in DMSO), and subsequently incubated for 72 h at 37 °C. Ultimately, inhibitory zone diameter (mean, in mm) was estimated, and for accuracy, measurement was carried out in a set of 3 replicates with the standard deviation of the mean values shown as error bars.

2.3.2. Antibacterial susceptibility test of α-aminophosphonate analogues

A dilution antibacterial susceptibility test was performed to estimate MIC values of different α-Amp compounds and standard drugs (kanamycin and streptomycin, as references) against target bacteria [52]. A 96-well microplate with an initial sample concentration of 150 μL of a 25 μg/mL solution in the first well of each row, followed by dilution of antibacterial agents (2 folds) using MB. A bacterial culture (1.5 μL) was then dropped into each well plate, realizing a final concentration of 7.5×10^4 CFU/mL. The wells were incubated at a speed of 100 rpm for 24 h at 37 °C, whereas MIC values for each bacterium were calculated by measuring OD600 (OD, optical density, measured at 600 nm, on final bacterial cultures): the lowest concentration of α-Amp compounds that showed the highest efficiency against planktonic cells provides the MIC values.

2.3.3. Biofilm formation inhibition assay

The crystal violet method was carried out to observe the biofilm formation inhibition in MB medium (2 wt% Glucose), with MIC or sub-MIC values (0.39, 0.78, 1.56, 3.13, 6.25, 12.5, 25, 50 and 100 μg/mL) of α-Amp compounds on a 96-well polystyrene microtiter plate. A final bacterial concentration of 7.5×10^4 CFU/mL was maintained by adding 1.5 μL of each bacterial culture suspension into each well. The positive control was a solution of each bacterial strain (150 μL, without the α-Amp$_s$), and the negative control was MB medium (150 μL) with MIC or sub-MIC of tested drugs. These microplates were incubated at 37 °C for 24 h and shaking rate of 100 rpm, followed by water removal and washing with double-distilled water (dd-H_2O) (3 times). The microplates were then stained with crystal violet (0.1%, 150 μL) and incubated at ambient temperature for 30 min, and subsequent washing to remove the stain excess. The stain was then dissolved in 33% (v/v) acetic acid (125 μL), followed by a 15 min incubation at ambient temperature. The OD was tested at 540 nm with the use of an EPOCH microplate spectrometer (BioTek, Instruments, Agilent, Santa Clara, CA, USA), and the percentage of eradication was calculated using Eq. 1:

$$\text{Eradication}\% = \frac{\text{OD positive } \textit{control} - \text{OD } \textit{sample}}{\text{OD positive } \textit{control}} \times 100 \quad (1)$$

2.3.4. Effect of α-aminophosphonate analogues on the mature biofilm

To examine the ability of α-Amp compounds to inhibit mature biofilm formation, 1.5 μL of bacterial suspension culture was distinctly injected into each well of 96-well flat-bottomed polystyrene microtiter plate (150 μL of MB medium, with 2 wt% $C_6H_{12}O_6$) to reach 7.5×10^4 CFU/mL, and then, it is similarly incubated (as mentioned in Section 2.3.2) for mature biofilm formation. Then, residues in each well were removed by pipetting and washed twice with dd-H_2O before adding MB medium with MIC and sub-MIC values (i.e., 3.13, 6.25, 12.5, 25, 50, 100, 200, and 400 μg/mL) of α-Amp compounds. It is challenging to find effective handling conditions for the inhibition of mature biofilm, especially when biofilm is formed; it requires special conditions like long contact time and large antibiotic concentrations (compared to free-floating planktonic cells). Similar procedures were used for positive and negative controls. Furthermore, each well content was removed, washed 2–3 times with dd-H_2O, and incubated in an oven at 60 °C for 1 h. Afterward, wells were stained with crystal violet, and eradication % was calculated using Eq. 1, as discussed in biofilm formation eradication. Experiments were performed in triplicate for the accuracy of measurements.

2.3.5. The effect of α-aminophosphonate analogues on the extracellular polymeric material formation

The same procedures (described in Section 2.3.4.) were followed to characterize these samples before crystal violet staining. A 200 μL of PBS was then used to wash the mature biofilms and stained separately with four dyes in the dark for 30 min. Fluorescein isothiocyanate was used to stain the carbohydrate of EPS components. DAPI (4,6-diamidino-2 phenylindole) was used to stain the nucleic acid, and SYPRO® Ruby was used to stain the majority of protein classes of bacterial cell membranes. SYTO 9 and propidium iodide were used to ensure the existence and extinction of bacterial cells. The cell conditions were determined after washing the matured biofilms with PBS to remove the excess stain following confocal imaging with a confocal microscope Leica TCS SP8 laser STED 3X (Leica, Wetzlar, Germany).

2.3.6. Morphological Evaluation of the Biofilms Eradication

The effects of α-Amp compounds on the morphology of bacterial cells were realized via SEM using the glutaraldehyde fixation technique for untreated and treated bacterial cell fixation. Strains of bacteria were isolated by centrifugation (13,000 xg) and subsequent incubation in glutaraldehyde (2.5%). Thereafter, the bacterial cells were dehydrated in an ethanol series of 30–100% for 5 min followed by their spread on a glass slide cover and analysis using JSM-7800 Prime, High-Resolution FE-SEM (JEOL Ltd., Tokyo, Japan).

2.3.7. Fluorometric determination of reactive oxygen species (ROS generation

The ROS effect was assessed in cells of *B. subtilis*, *E. coli*, and *P. aeruginosa* that had been treated with synthetic antibacterial drugs for a period of 24 h. The untreated cells served as a control for the experiment. After collecting the samples, they were centrifuged for five minutes at a speed of 10,000 rpm. Before being treated with 2′,7′-dichlorofluorescin diacetate (DCFH-DA), the supernatants were diluted by a factor of 10,000 in PBS. This was done under the ROS Assay Kit that was purchased from the Beyotime Institute of Biotechnology in Haimen, China. In the end, the microplate was left to sit in an incubator for 30 min at a temperature of 37 °C. For data collection at 488 nm, a Spectra Max M5 Multi-Mode MicroPlate Reader manufactured by Molecular Devices in California, USA was utilized.

2.3.8. Effect of α-aminophosphonate on recombinant green fluorescent protein (GFP expression

Electrocompetent cells of *B. subtilis*, *E. coli*, and *P. aeruginosa* were subjected to transfection using the expression vector pSEVA234 harboring the green fluorescent protein (GFP) gene (pSEVA234-GFP) using the process of electroporation [51]. The colonies that underwent successful transformation were collected from LB-agar plates and subsequently cultivated in LB liquid medium at a temperature of 37 °C until they reached the mid-logarithmic growth phase. A phosphate-buffered saline (PBS) solution, supplemented with 10% Luria-Bertani (LB) medium, was employed for the cultivation of the tested cells harboring pSEVA234-GFP until reaching an optical density at 600 nm (OD600) of 0.2. Subsequently, α-Amp compound [B] was introduced to the culture at doses of 3.13 μg/mL and 1.57 μg/mL for *B. subtilis*, *E. coli*, and *P. aeruginosa* cells. The culture was then incubated for a duration of 30 min. The induction of recombinant GFP expression was achieved by the addition of isopropyl β-D-1-thiogalactopyranoside (IPTG) at a concentration of 0.5 mM. Subsequently, the cultures were cultivated at a temperature of 30 °C overnight duration. The cells of tested microbials were collected using the process of centrifugation, after which the liquid portion above the sediment, known as the supernatant, was removed and discarded. The cells that were gathered were suspended in phosphate-buffered saline, subjected to lysis using sonication, and the resulting supernatants were obtained following centrifugation. The expression of GFP was detected using SDS-PAGE and Spectra Max M5 Multi-Mode MicroPlate Reader.

2.4. Molecular docking assessment

To gain insight into the mechanisms of attraction, binding orientations, spatial separation, and the strength of the bond formed between these compounds and the protein structures, an investigation into the molecular interactions between three synthesized compounds and three bacterial proteins was carried out. Molecular operating environment (MOE) software was used to illustrate the docking of α-Amp analogues on bacterial proteins [32]. Proteins from three distinct types of bacteria (*B. subtilis*, *E. coli,* and *P. aeruginosa*) were retrieved from a protein data bank (pdb codes: 2FQT, 6YD9, and 3HEM) for modeling [36,54]. The proteins chosen for molecular docking were selected based on their biological importance, the presence of experimentally confirmed structural data, a high-resolution and straightforward 3D structure, their suitability for drug development, and their critical involvement in the disease pathway. These criteria were employed to establish a strong basis for conducting comprehensive studies on the interactions between ligands and proteins. Partial charge calculations, 3D protonation, correction of strands, and energy minimization were analyzed to configure the interaction between ligand proteins [18]. Induced-fit docking was chosen for its ability to utilize active ligand location as a placement guide. Pharmacophore annotations were excluded with database examination in mdb format. Energy minimization gradient was 0.05, and MMFF94X was the default force field [19].

3. Results and discussion

3.1. Synthesized α-Amp analogues identification

A simple green one-pot method was used to produce different analogues types of α-Amps. Table S1 reports the types (among aldehydes, amines, and phosphite) and ratios of precursors selected for synthesizing seven analogues of α-Amp ([A] to [G] samples); CH_3CN was used as the reaction solvent, while the IL (as reaction catalyst) content was set at 20% of the mmol IL. The table also reports the amount of IL and the yield of relevant reactions (between 68% and 76.3%). The recommended reaction mechanism for α-Amp analogues preparation is displayed in Scheme 1, describing the first step is the formation of an imine-intermediate, which is then nucleophile attacked the carbon atom of amin by an electron-rich source of phosphorus that could lead to the production of phosphonium ion. The IL Lewis acid catalyzes this reaction [44]. In the last stage, the interaction of phosphonium intermediates with water facilitates the release of phenol, leading to the formation of specific α-Amp analogues. In brief, the compound [A] was prepared using salicylaldehyde, diethylenetriamine, and triphenyl phosphite with 1.90 mmol IL, while for preparation of compound [B], benzaldehyde, ethylenediamine monohydrate, and triphenyl phosphite were used with 3.31 mmol IL; for obtaining compound [C], we used the same aldehyde and phosphite of compound [B] but used glucosamine instead and 1.86 mmol IL; also on the same path, compound [D] was synthesized using urea and 3.27 mmole IL; compound [E] was obtained by using p-phthalaldehyde, *tert*-butyl carbamate, and trimethyl phosphite precursors with 1.40 mmol IL; same as compounds [E], and [F] were prepared with p-phthalaldehyde and trimethyl phosphite as an aldehyde and phosphite sources with only change of urea as amine source with 3.27 mmol IL, and lastly for preparation of compound [G], urea, and trimethyl phosphite were used as a compound [F], but using glutaraldehyde as aldehyde source instead with 3.27 mmol IL. Notably, the yield of the as-prepared compounds was obtained at around 70% after the reaction. Furthermore, a possible crystalline structure of α-Amp analogues is provided in Fig. 1 and Table S2 for a detailed structural understanding of these analogues.

3.1.1. Spectroscopic characterization of the analogues

FT-IR analysis was carried out to identify and determine the functional groups on prepared α-Amp analogues. Fig. 2 and Fig. S1 illustrate

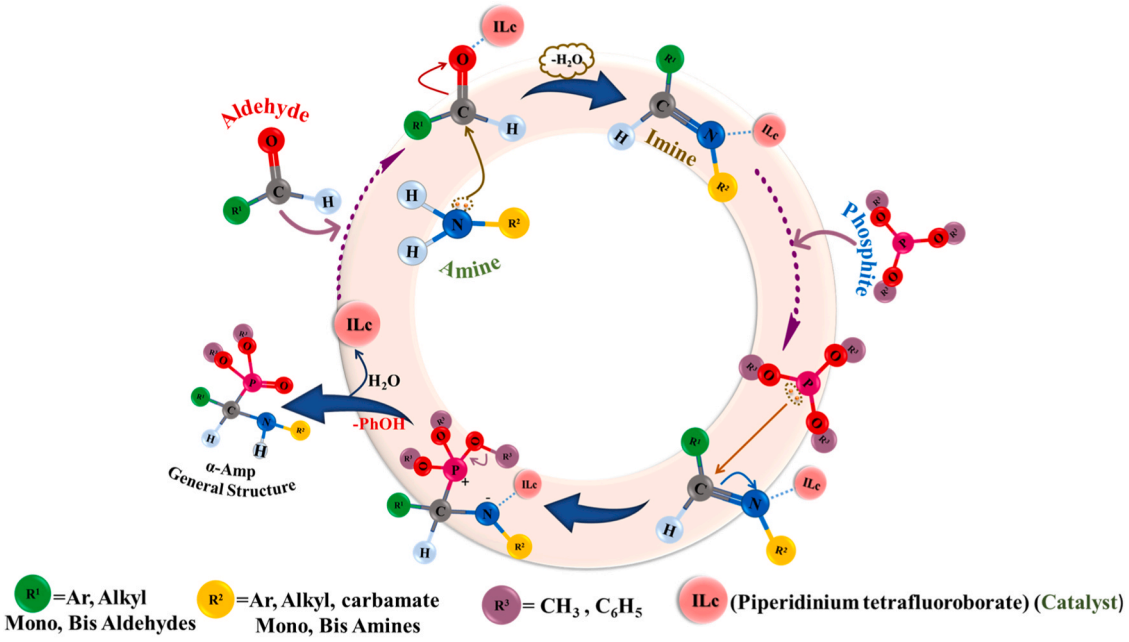

Scheme 1. Recommended reaction mechanism for α-Amp analogues preparation.

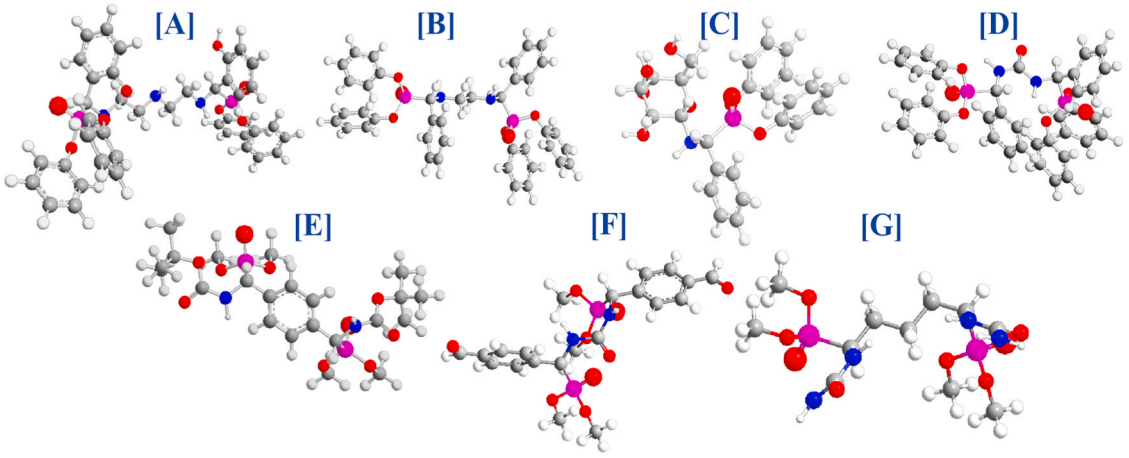

Fig. 1. Possible molecular structural illustration of resulting α-Amp analogues.

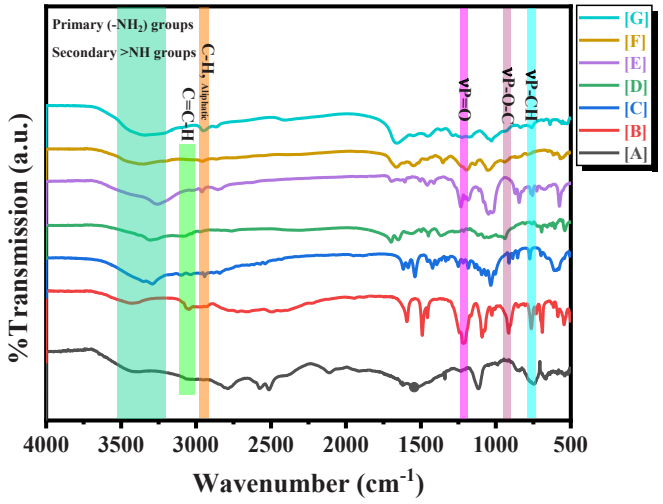

Fig. 2. Obtained FT-IR spectra of resulting α-Amp analogues.

the distinct vibrations of each compound. Besides, the NMR analysis was conducted to confirm the structure of the resulting analogues. Notably, DMSO-d_6 solvent is used to identify the ^{1}H NMR (600 MHz), ^{31}P NMR (243 MHz), and ^{13}C NMR (150 MHz), and their related peaks for each compound are displayed in Fig. S2. FT-IR and NMR analysis reveal the presence of prominent peaks for each compound as:

[A] :diphenyl ((R)-((2-((2-((((S)-(diphenoxyphosphoryl)(2-hydroxyphenyl)methyl)amino)ethyl)amino)ethyl)amino)(2-hydroxyphenyl)methyl)phosphonate

Yield: 73.5%, FT-IR: cm^{-1} = 3429 (NH str.), 3300–2350 (OH str.) broad peak, 3061 (C═C-H str.), 2729 (C-H str.) aliphatic, 1593 (NH bend.), 1490 (C═C str., C-H aromatic), 1458 (OH bend.), 1378 (C-H str.), 1216 (P = O), br., 1072 (P-O-C), 915 (P-C), and 757 (C-H) bend. Imam et al., [31,42,68]. **^{1}H NMR**: δ ppm = 3.14 (br. m, 4 H, 2CH_2-NH), 3.32 (br., 4 H, 2CH_2-NH), 4.20 (broad, 22 H, P-C-H chiral), 4,62 (br., N-H), 7.55 (br. 2 H, 2NH), 6.74 ~ 7.39 (m, 28 H, Ar-H), 10.27 (br, 2 H, 2OH); **^{13}C NMR**: Ar-C-O-P appear at δ = 157.86. These carbons also show up as several peaks in the instance of Ar (8 C) in phenyl ether around δ = 115.70, 119.10, and 129.80 ppm. Ar-CH in hydroxy phenyl appears as multiple peaks at δ = 123.30, 121.80, and 120.90 ppm.

Chiral carbons (2 P-C) appear at δ = 50.28 and 51.15 ppm. For ethylene carbons in -HN-CH_2CH_2-, the strong and high-intensity peaks appear in the range of δ = 43.48 and 44.85 ppm [44], denoting that the unexpectedly high intensity of the ethylene peak, and also suggests a non-stoichiometric compound; **^{31}P NMR**: indicates the presence of the phosphonate component as broad P(O) signal at δ = 25.53 ppm [47].

[B]: diphenyl ((R-((2-(((S-(diphenoxyphosphoryl(phenyl methylaminoethylamino(phenylmethylphosphonate

Yield: 71.42%, FT-IR: cm^{-1} = 3433 (NH, str.) wide peak, 3049 (C═CH, str.) benzene ring, 2753 (CH, str.) aliphatic, 1593 (NH, bending), 1491 (C═C, str.) phenyl ring, 1220 (P = O) broad peak, 1092 (P-O-C), 915 (P-C), and 763 (C-H) bending [31,42,44]. **^{1}H NMR**: δ ppm = 3.09–3.18 ppm (m, 4 H, $2CH_2$), 3.91 (broad, 2 H, NH), while protons on chiral carbon of (P-C-H) appear at δ = 4.66 ppm as broad multiplet peak for (2 H). In addition, the aromatic part shows different multiplet peaks as (3 H, Ar-H) that appear at δ = 6.78 ppm as a triplet with (m, 4 H, C_{Ar}-H) at δ = 6.85 ppm, (m, 15 H, C_{Ar}-H) at δ = 7.37 ppm, and (m, 8 H, C_{Ar}-H) at δ = 7.92 ppm. These multiplet peaks are characterized by a coupling constant ($^{1}J_{PC}$ = 7.8, 9.6, 8.9, and 9 Hz); **^{13}C NMR**: shows different shifted peaks, which indicate the appearance of Ar-C-O-P peak that appears at δ = 157.96, while the other peaks for Ar-O-P and Ar-CH-appeared at δ ppm = 115.70, 119.20, 123.18, 126.38, 128.80, 131.10, and 151.41 ppm. While (2 P-CH-) chiral carbon appeared at δ = 55.57, 57.32 ppm, and -CH_2-NH at δ = 44.05 ppm; **^{31}P NMR**: shows the presence of the phosphonate component associated with the α-aminophosphonate ester at δ = 16.99 ppm [65].

[C]: diphenyl ((R-phenyl(((2 S,3 R,4 S,5 S,6 R—3,4,5-trihydroxy-6-(hydroxymethyltetrahydro-2 H-pyran-2-ylamino methylphosphonate

Yield: 71.68%, FT-IR: cm^{-1} = 3292 (NH str.) large peak, 3038 (C═C-H str.) benzene ring, 2943 (C-H str.) aliphatic, 1617 (NH, bend.), 1540 (C═C str.) phenyl group, 1458 (OH) bend., 1422 (C-O) bend., 1184 (P = O) broad peak, 1034 (P-O-C), 912 (P-C), and 774 (C-H) bend. Imam et al., [31,42,68]. **^{1}H NMR**: The methylene and methine peaks are observed at δ = 3.17 ppm (m, 2 H, CH_2), 3.45–3.66 (m, 5 H, 5-CH pyran ring. 4.7 (d,1 H, *J* = 24 Hz. CH chiral), 5.25 (br. 4 OH,) 7.13 (br. M, 3 H, Ar-H), 8.08 (br. M., 12 H, Ar-H), 9.10 (br., 1 H, NH). **^{13}C NMR**: Ar-C-O-P appear at δ = 157.85 ppm (2 C). The (Ar-C) appears at δ = 129.76 (2 C), 119.17 (2 C), 115.72 (2 C) ppm. (N-CH-O) appears at δ = 93.43 ppm, while (O-CH-CH_2OH) at δ = 89.27 ppm. Additionally, the peaks of cyclo hexane appear at δ = 77.48, 72.77, and 70.20 ppm. The (CH_2OH) peak appears at δ = 61.03 ppm, the chiral carbon (P-CH) appears at δ = 54.98, 57.92 ppm; **^{31}P NMR**, indicates the presence of the phosphonate component at δ = 14.82, and 19.55 ppm [12]. The duplet (P) peaks as the compound are a mix of diastereomers.

[D]: diphenyl ((S-(3-((R-(diphenoxyphosphoryl(phenyl methylureido(phenylmethylphosphonate

Yield: 67.98%, FT-IR: cm^{-1} = 3305 (NH str.) broad peak, 3053 (C═C-H str.) benzene ring, 2764 (C-H) aliphatic, 1698 (C═O str.), 1650 (NH) bending, 1558 (C═C str.) phenyl group, 1364 (C-N str.), 1215 (P = O) broad peak, 1074 (P-O-C), 940 (P-C), 806 (C-H) bending [42,48]. **^{1}H NMR**: 2 H of (P-C-H) chiral carbons appear as a multiplet at δ = 5.76 ppm and δ = 8.56 ppm (br., 2 H, NH), additionally, the aromatic protons found as multiplet in the range δ = 6.75–7.43 ppm; **^{13}C NMR**: for C═O appear at δ = 157.80 ppm, and C_{Ar}-O appear at δ = 115.76, 119.29, 125.01, 128.36, 130.21, 141.30, 146.26, and 153.88 ppm. The structure modification is identified by the presence of a chiral carbon atom as (P-C) at δ = 51.80 ppm. **^{31}P NMR**: shows the appearance of the phosphonate component peaks at δ = 18.11 ppm [12].

[E]: di-tert-butyl ((1 R,1′R—1,4-phenylenebis((dimethoxyphosphorylmethylenedicarbamate

Yield: 76.29%, FT-IR cm^{-1} = 3255 (NH str.) wide peak, 3030 (C═C-H str.) benzene ring, 2961, and 2844 indicate (C-H) aliphatic, 1697 (C═O str.), 1607 (N-H) bending, 1504 (C═C str.) phenyl group, 1457 (C-N str.), 1234 (P = O) broad peak, 1049 (P-O-C), 1024 (C-O str.), 869 (P-C), and 844 (C-H) [42,48]. **^{1}H NMR**: *Tert*-butyl peak appeared at δ = 1.36 ppm (s, 18 H, CH_3) with unexpectedly low intensity. It can be speculated by the hydrolysis or oxidation reaction of the *tert*-butyl group yielding acrylic acid or acetate. The methoxy groups appear at δ = 3.61 ppm (m, 12 H, 4(O-CH_3)). The methine (2 H, P-CH) peak appears at δ = 5.0 ppm (m, 2 H, CH). The phenyl peak appears at 7.40 ppm (s, 4 H, CH_{Ar}). **^{13}C NMR**: Carboxyl carbon appears at δ = 145.73, while Ar-C appears at δ = 127.32–138.0 ppm. The *tert*--carbon appears at δ = 68.63–69.78 ppm. The chiral carbon (2-P-C) appears at δ = 53.79 ppm, and the methoxy (3(O-CH_3)) appears at δ = 53.23 ppm. The *tert*-butyl carbons (3(CH_3) peaks are observed at δ = 28.76 ppm; **^{31}P NMR**: shows phosphonate moiety (P (O)) at δ = 23.51, and 23.85 ppm [34], as this compound is diastereomer with two-chiral centers.

[F]: dimethyl ((R)-(3-((S)-(dimethoxyphosphoryl)(4-formylphenyl)methyl)ureido)(4-formylphenyl)methyl)phosphonate

Yield: 70.40%, FT-IR: cm^{-1} = 3355 (NH str.) large peak, 3035 (C═C-H str.) broad peak, 2958, and 2845 for (C-H) aliphatic, 1720–1610 [broad, (C═O str.), and (NH, bending)], 1550 (C═C, str.) phenyl group, 1353 (C-N str.), 1196 (P = O) broad peak, 1053 (P-O-C), 941 (P-C), and 788 (C-H) [44,48]. **^{1}H NMR**: Methoxy groups (12 H, 4(O-CH_3)) appear as multiplet at δ = 3.51 ppm, for (2 H, P-C-H) as multiplet at δ = 5.08 ppm, aromatic groups shown as multiplet at δ = 7.41 ppm, (N-H, 2 H) appears at δ = 8.42, and 9.23 ppm as a broad peak, and aldehyde proton of (HC═O) at δ = 10.02 ppm; **^{13}C NMR**: Aldehyde peak (HC═O) appears at δ = 191.23 ppm, while the peak at δ = 161.04 ppm for the carbonyl group of urea. The aromatic carbon that's directly attached to an aldehyde (C_{Ar})-C═O appears at δ = 143.54–144.04 ppm, While Ar-C appears at δ = 116.44, 118.20, 125.80, and 127.60 ppm. The methoxy and chiral carbon overlapped in the range of δ = 51.29–52.72 ppm; **^{31}P NMR**: shows the presence of phosphonate component (P (O)) at δ = 33.03 ppm [34].

[G]: tetramethyl ((1S,5S)—1,5-diureidopentane-1,5-diyl)bis (phosphonate)

Yield: 72.5%, FT-IR: cm^{-1} = 3385 (NH str.) broad peak, 3195 (NH_2 str.), 2962, and 2859 for (C-H) aliphatic, 1667 (C═O str.), 1605 (NH) bending, 1351 (C-N str.), 1196 (P = O) broad peak, 1057 (P-O-C), 920 (P-C), and 793 (C-H) [42,48]. The multiplet peak of (m, 6 H, $3CH_2$) is observed at δ = 1.07 ppm. The broad methoxy peaks of (12 H, O-CH_3) appear at δ = 3.48 ppm, (2 H, P-C-H) appear at δ = 4.69 ppm. The broad amine peaks of (2 H, NH) appear at δ = 5.71 ppm; **^{13}C NMR**: The carbonyl peak appears at δ = 161.0 ppm. The methoxy groups appear at δ = 52.81 ppm and chiral carbon (P-C) at δ = 51.19 ppm. The butylene peak (-$CH_2CH_2CH_2$-) is observed at δ = 18.90 ppm; **^{31}P NMR** shows the existence of the phosphonate moiety associated with the P (O) as a doublet at δ = 33.02 ppm [65].

In addition to nuclear magnetic resonance (NMR) spectroscopy, high-performance liquid chromatography (HPLC) analyses were performed to determine the degree of purity of the suggested substances. As depicted in Fig. S3, the synthesized molecule exhibits a distinct peak corresponding to the chemical composition of α-aminophosphonate moieties, without the presence of other pronounced peaks. The observed relationship between peak area and size, when comparing the main peak to smaller peaks, indicates that the compound being analyzed has a purity around 95%. This suggests that the compound is suitable for usage without requiring additional purification steps.

4. Antibacterial characteristics of α-Amp analogues

4.1. Modified Kirby-Bauer antibacterial susceptibility test

The antibacterial activity of α-Amp analogues was studied against the planktonic forms of targeted bacteria. The concentration of reference drugs was chosen as per the standard of World Health Organization (WHO). First, the inhibition zones (diameter-based) were determined for each compound separately against targeted bacteria to highlight the

antibacterial efficacy of each compound, as presented in Fig. 3. In Table 1, among different synthesized compounds, compounds [B], [D], and [G] reveal the most efficient antibacterial agents with inhibition zones ranging from 41 to 37 mm for *E. coli*, 39–30 mm for *P. aeruginosa,* and 28–23 mm for *B. subtilis*. Conversely, the efficiency of compounds [A], [C], [E], and [F] correspond to inhibition zones of 20–12 mm for *E. coli*, 23–10 mm for *P. aeruginosa*, and 13–8 mm for *B. subtilis*. For comparison, two reference drugs, kanamycin, and streptomycin were used [21]. As shown in Table 1, the inhibition zone diameter, when kanamycin (30 μg) was used as a reference drug, reached 25 mm for *E. coli*, 30 mm for *P.aeruginosa,* and 22 mm for *B. subtilis*. In comparison, streptomycin (10 μg) showed inhibition zones of 24 mm for *E. coli*, *B. subtilis*, and 22 mm for *P.aeruginosa*. Therefore, compounds [B], [D], and [G] show more efficient than conventional commercial antibacterial agents; this could be due to the existence of amine and carboxyl groups on the cell surface of pathogens and the greater affinity of α-Amp analogues toward these groups [46,62]. ,

4.2. MIC values of α-Amp analogues

The synthesized α-Amp compounds were tested for inhibiting the growth of targeted bacteria planktonic cells. All the prepared compounds were tested in vitro, in parallel with kanamycin and streptomycin. In Table 2, compound [B] shows the highest antibacterial efficiency compared to the other α-Amp analogues against each targeted bacterium. The MIC values of compound [B] are as low as 3.13 μg/mL for *E. coli* and *P. aeruginosa,* and 6.25 μg/mL for *B. subtilis*. In contrast, kanamycin shows MIC values of 46.9 μg/mL for *E. coli*, 64 μg/mL for *P. aeruginosa*, *and* 23.4 μg/mL for *B. subtilis*, while for streptomycin the values increase to 187 μg/mL for *E. coli*, 93 μg/mL for *P. aeruginosa*, and 23.4 μg/mL for *B. subtilis*. Notably, compounds [B], [D], and [G] have the same MIC value for *E. coli* planktonic cells (i.e., 3.13 μg/mL). Similarly, compounds [A], [C], and [F] show the same MIC value for *E. coli* planktonic cells (i.e., 50 μg/mL, comparable to kanamycin). However, the MIC for compound [E] reaches an intermediary value (i.e., 25 μg/mL); this might be related to the presence of functional amines and carboxyl groups on the cell surface of pathogens. For *P. aeruginosa* planktonic cells inhibition, compounds [B], [D], and [G] show high activity with MIC values close to 3.13, 12.5, and 6.25 μg/mL, respectively, while the MIC value is close to 50 μg/mL for compounds [C] and [F]. In addition, the MIC value for compound [A] increases up to 100 μg/mL, while for [E], the MIC is close to 25 μg/mL. It can be noticed that compounds [B], [D], and [G] showed similar promising antibacterial activity for *B. subtilis* planktonic cell inhibition (consistently the two other bacterial strains). In contrast, the other antibacterial agents (including commercial compounds) show higher MIC values than compounds [B], [D], and [G]. This comparison confirms that compounds [B], [D], and [G] have the highest antibacterial activity against other α-Amp analogues and reference drugs (kanamycin, and streptomycin). This strong suppression could be attributed to the ortho-hydroxyl group that forms intramolecular phosphorous bonds within the aromatic aldehydes, which enhances the antibacterial action. These aldehydes have been shown to impede the growth of bacteria. It was previously established that ortho–OH groups have a significant inhibiting impact. Hence, Friedman and coauthors correlated, among different samples, the best performance of benzaldehydes, benzoic acids,

Table 1
Zones of inhibition (mm) for antibacterial activity of synthesized α-Amp analogues on clinical pathogens, compared with standard commercial antibiotics.

α-Amp$_s$ and reference drugs	Inhibition zones diameter (mm)		
	E. coli	*P. aeruginosa*	*B. subtilis*
[A] (25 μg)	12	10	8
[B] (25 μg)	41	39	28
[C] (25 μg)	11	15	10
[D] (25 μg)	40	30	25
[E] (25 μg)	20	23	13
[F] (25 μg)	13	18	12
[G] (25 μg)	37	35	23
Kanamycin (30 μg)	25	30	22
Streptomycin (10 μg)	24	22	24

Table 2
MIC values (μg/mL) of the synthesized α-Amp analogues against the planktonic forms of tested bacteria.

Compounds	Microorganisms MIC (μg/mL)		
	E. coli	*P. aeruginosa*	*B. subtilis*
[A]	50	100	100
[B]	3.13	3.13	6.25
[C]	50	50	100
[D]	3.13	12.5	6.25
[E]	25	25	50
[F]	50	50	50
[G]	3.13	6.25	12.5
Kanamycin	$\geq$ 46.9	$\geq$ 64	$\geq$ 23.4
Streptomycin	$\geq$ 187	$\geq$ 93	$\geq$ 23.4

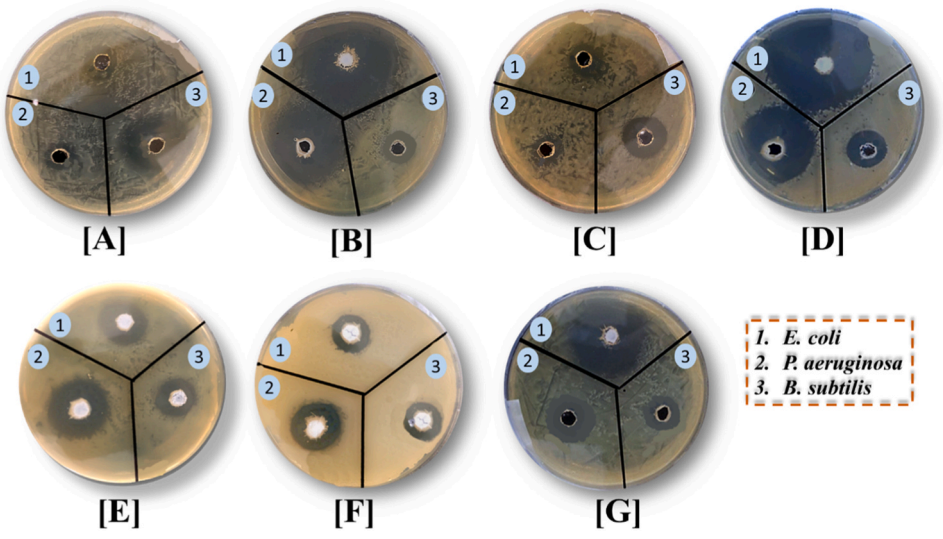

Fig. 3. Images of antibacterial assessment through agar disc diffusion method against each targeted bacteria in planktonic form.

and benzoic acid methyl ester against four microbes to the presence of ortho-hydroxyl moieties [25]. Besides, their observation further revealed that -OH groups were more active than -OCH_3 groups. Such observation confirms the higher antibacterial activity of compounds [B], [D], and [G] compared to the other prepared compounds in relation to the presence of -OPH group. Conversely, the presence of –OCH_3 moieties in compounds [E] and [F] can explain their weaker antibacterial effect.

4.3. *Biofilm formation inhibition*

Bacterial biofilm represents a complex community of microorganisms that adhere to biotic or abiotic surfaces [30]. Biofilms commonly form on moist surfaces, particularly those found in water pipelines. Synthesized α-Amp analogues were used to test their deformation ability for biofilm eradication. The reaction was studied after a fixed incubation time (i.e., 24 h) while applying MIC and sub-MIC concentrations. The biofilm deformation activity (quantified as eradication percentage) allows classifying the α-Amp analogues into two groups: (1) compounds [A], [B], and [C] (Fig. 4**a**), while (2) include compounds [D], [E], [F], and [G] (Fig. 4**b**). Fig. 4**c** shows the microplate wells before and after the treatment with the α-Amp analogues; the treatment is associated with a decrease in the color, which, in turn, indicates a higher deformation activity compared with untreated particles (control test). The results in Fig. 4**a** indicate that the most significant inhibition percentage is

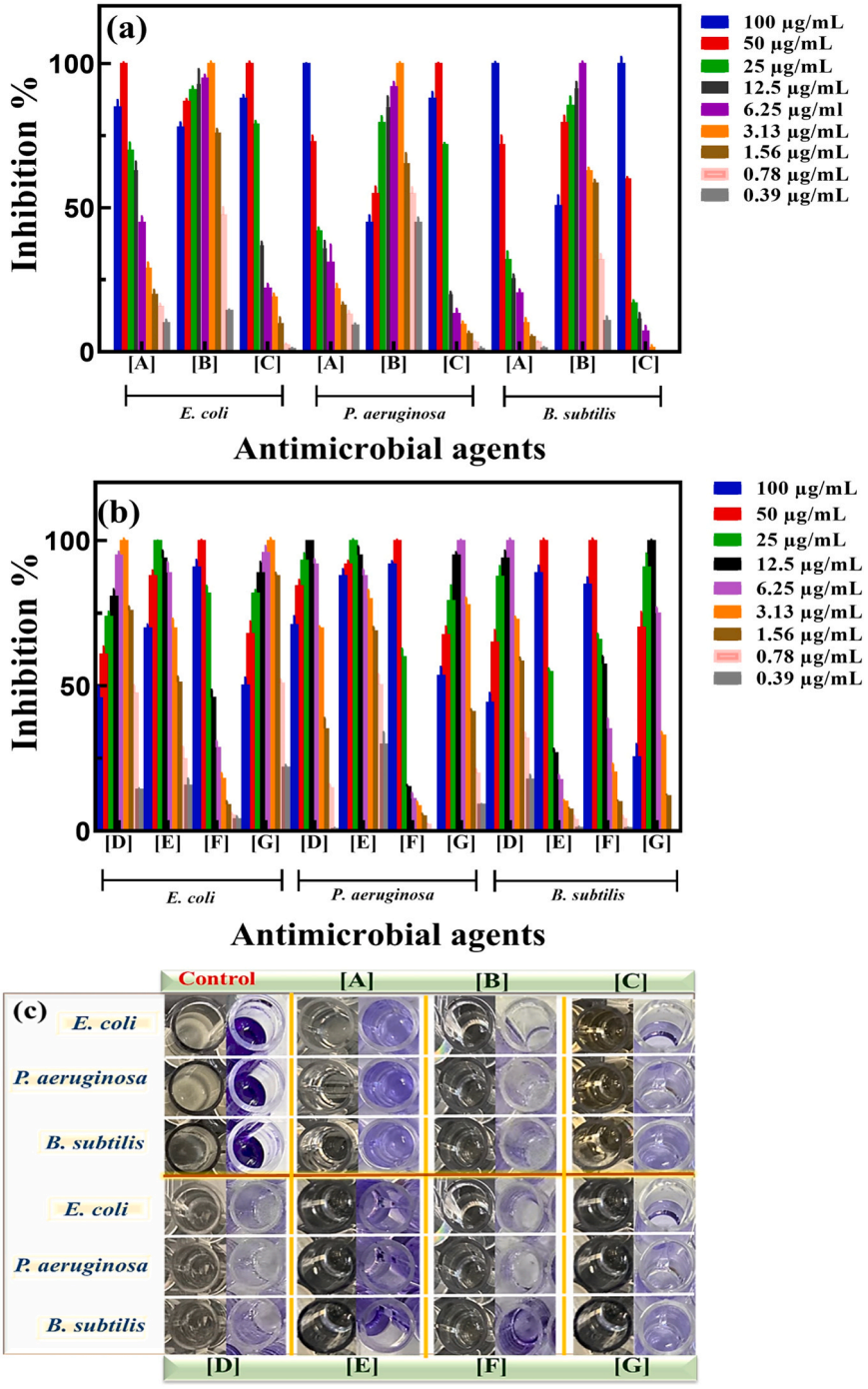

Fig. 4. (a, b) Inhibition of biofilm formation for targeted bacteria at MIC and sub-MIC values for α-Amp analogues. (c) The real images of microplate wells before and after the treatment with the α-Amp analogues.

achieved by compound [B], which shows 100% biofilm inhibition for tested bacteria at concentrations ranging from 3.13– 6.25 μg/mL. In contrast, compound [A] requires a higher drug dosage of 50 μg/mL for *E. coli* and 100 μg/mL for *P. aeruginosa* at 100% inhibition level, while 100 μg/mL for *B. subtilis* at 99% level. Besides, for compound [C], a 100% inhibition percentage for gram negative bacteria is attained at 50 μg/mL and 100 μg/mL, respectively, while the inhibition percentage for *P. aeruginosa* biofilms reaches 98% at 50 μg/mL concentration. In Fig. 4**b**, compounds [D] and [G] show a 100% inhibition effect for all tested bacteria in the concentrations range of 3.13–12.5 μg/mL. Furthermore, the compound [E] shows 100% inhibition efficiency for only *E. coli* at 25 μg/mL and 98% inhibition efficiency for *P. aeruginosa* (25 μg/mL) and *B. subtilis* (50 μg/mL), respectively. Finally, the compound [F] shows that the inhibition percentage for all tested bacteria could reach around 99%, at 50 μg/mL concentration. The inhibition effect for biofilm formation can be associated with the cationic and anionic characteristics of the α-Amp analogues, which inhibit the bacterial cells from sticking to the surface of the plates [20]. Additionally, the chemical structure of phosphide compounds may promote electrostatic exchanges with bacteria's surface charge species, forming phospholipid membranes. Amphipathic structure can also hinder membrane-water interactions. The typical inhibition percentage surpasses 98% at optimal concentrations.

4.4. Mature biofilm eradication

After inhibiting biofilm formation, eradicating mature films (already coating active surfaces) is crucial for preventing pollution and health. As

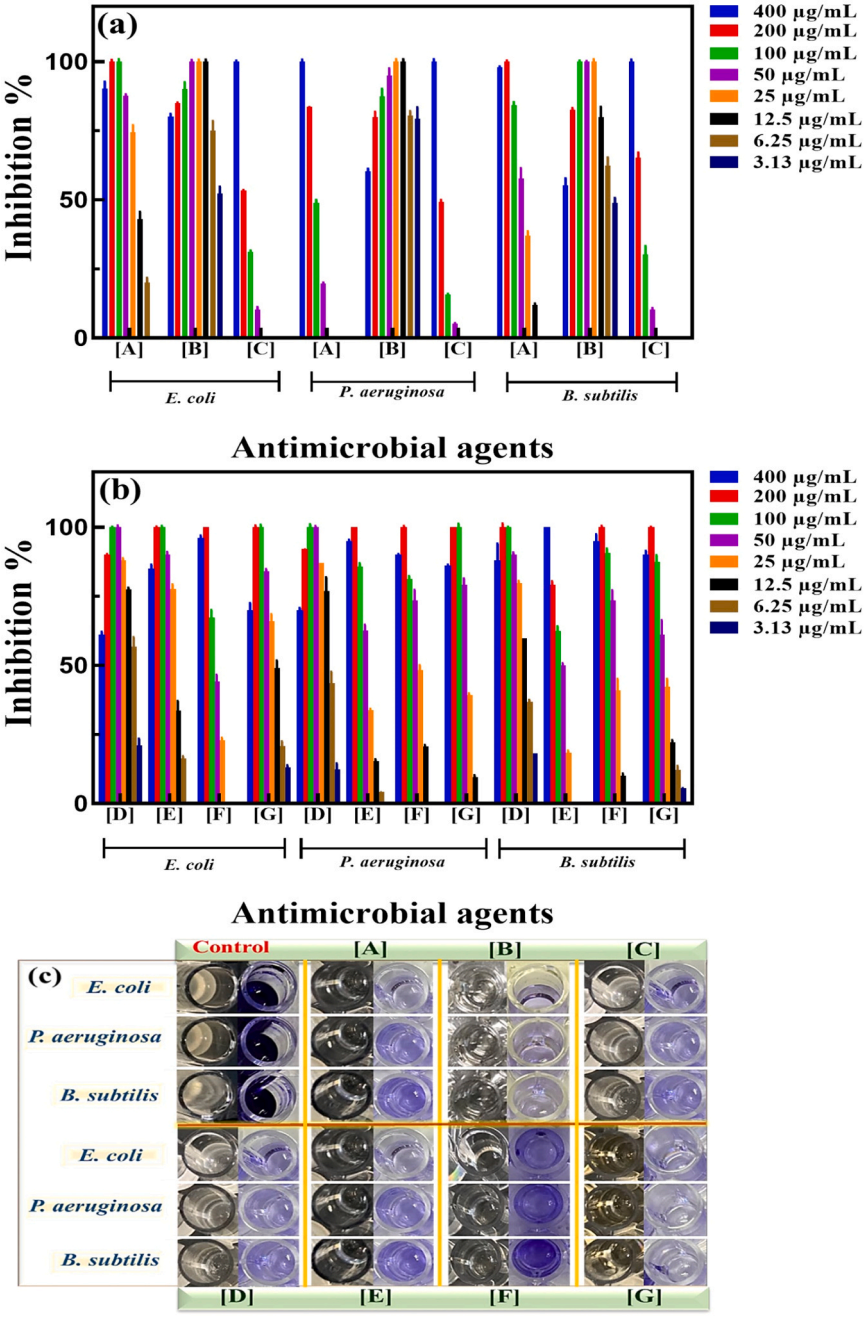

Fig. 5. (a, b) Mature biofilm eradication by MIC and super-MIC values of α-Amp compounds against targeted bacteria, and (c) Micro-plate images showing the dye intensity differences between the fully eradicated and non-eradicated bacterial biofilms.

noted, mature biofilm removal needed concentrations above MIC. Each studied bacteria's mature biofilm removal effectiveness is shown in Fig. 5. Similar to the preceding section, α-Amp compounds are split into two classes. Fig. 5**a** indicates compound [A-C] eradication efficiency. Compound [B] is most effective, preventing mature biofilms at 12.5, 12.5, and 25 μg/mL for *E. coli*, *P. aeruginosa*, and *B. subtilis*, respectively. Higher concentrations are necessary for compound [A]; the concentration limit strongly depends on the type of microorganisms: 100 μg/mL for *E. coli*, 200 μg/mL for *B. subtilis* biofilms, and up to 400 μg/mL in the case of *P. aeruginosa* biofilm. For compound [C], the concentration limit increased to 400 μg/mL (independently of the type of microorganism). Fig. 5**b** summarizes the effect of the addition of compounds [D-G] on the eradication efficiency of formed biofilms. These compounds eradicate the mature biofilms of bacteria when higher MIC values are used. Compound [D] eradicated 100% of the mature biofilms of *E. coli* and *P. aeruginosa* at concentrations of 50 and 100 μg/mL, respectively, while *B. subtilis* biofilms were 100% eradicated at concentrations of 100 and 200 μg/mL. Compound [G] showed a similar effect to compound [D], where eradication efficiency for bacterial biofilms reached 100% at a drug concentration ranging from 100 to 200 μg/mL. Compound [E] showed a 100% eradication effect for mature biofilms of *E. coli* at 100 μg/mL, whereas *P. aeruginosa* biofilm exhibited 100% eradication efficiency at 200 μg/mL, and *B. subtilis* biofilms at 400 μg/mL. Furthermore, at 200 μg/mL concentration, compound [F] eradicated each tested bacteria's mature biofilms by 100%. Fig. 5**c** shows the microplate wells before and after the treatment with α-Amp compounds. The lower color intensity demonstrates higher deformation activity than untreated particles (control wells). There is a correlation between the unique nature of α-Amp compounds, which can be either cationic or anionic, and the high activity of these compounds, which allows them to interact with both gram-negative and gram-positive bacteria. As a result, this might improve the binding to the phospholipid membrane, which would result in the production of an amphipathic structure. This change speeds up the process of adjusting at the interfaces between the membrane and the water, which ultimately results in a fatal consequence due to the increased permeability of the bacterial cell [20,51].

SEM analysis, Fig. 6**,** shows the fatal effect of α-Amp compounds against targeted bacterial cells. Herein, Fig. 6 **(g-i, (m-o,** and **(v-x** indicate the high lethal effect of compound [B], **(m-o** compound [D], and **(v-x** compound [G], respectively. This higher activity is highlighted by the comparison with the control, untreated bacteria, in Fig. 6 **(a-c**. The effective binding of amino phosphonic boosts the lethal depolarization of cell membrane and generates a hollow path to promote the leakage of bacterial cells [28]. In addition, Fig. 6 **(j-i)** and **(s-u)** indicate the substantial lethal effect for compound [C] and Fig. 6 **(s-u)** compound [F], respectively, on the bacterial cell membrane. In contrast, the lethal effect slightly decreased for compounds [A] and [E]. Compound [A], Fig. 6 **(d-f)**, and compound [E], Fig. 6 **(p-r)**, showed an aggregation behavior that could be a result of the strong binding of antibacterial agent to the bacterial membrane. The differences between α-Amp analogues and control experiments can be directly associated with reactive oxygen species (ROS) that generate electrostatic contact between the positively and negatively charged points in the α-Amp_s/bacterial surface systems. Previous studies have provided evidence of the presence of nucleobases in α-Amp_s, which exhibit promising biological properties [11]. Moreover, α-Amp_s have the potential to induce disruption through direct contact with the surface of bacteria. The interaction between the contact and the microenvironment in the vicinity of bacteria α-Amp_s will result in the production of reactive oxygen species (ROS), which, in turn, induce damage to bacterial cells. The observed damage can arise from the cleavage of peptide bonds or the formation of cross-linked derivatives between proteins through a reaction involving carbon-centered radicals. These radicals have the ability to interact with DNA molecules, resulting in the binding of the radicals to the nucleic acid strands. Consequently, this binding disrupts the helical structure of DNA and leads to the destruction and disintegration of the biochemical processes involved. The occurrence of a cyclic redox reaction resulting from this damage gives rise to the generation of several hydroxyl radicals in proximity to the binding site, hence causing various forms of DNA damage. The embodied bacterial charge surface with α-Amp_s caused intermittent electron transport across cellular trans-membranes. Cationic/anionic α-Amp_s may cause membrane perturbation via inducing ROS. This emphasizes the significance of α-Amp_s rich in functional groups (such as NH, P = O, C═O, and OH) that trigger the generation of ROS to damage several biological components, including nucleic acids, and proteins, as well as bacterial cell membrane.

To study the bacterial cell disruption by ROS formation, tested cells were treated with the produced antibacterial compounds (Fig. 7). ROS level was recorded at the greatest value after treatment with the compound [B] in comparison with other produced compounds, and the control. This could be due to the electrostatic interaction between active charge surface of resultant chemicals and microbial surface that led to intermittent electron transfer across cellular trans-membranes. Rowe-Magnus et al. reported that charge active chemical could cause membrane disturbance via ROS induction [49]. This shows the relevance of

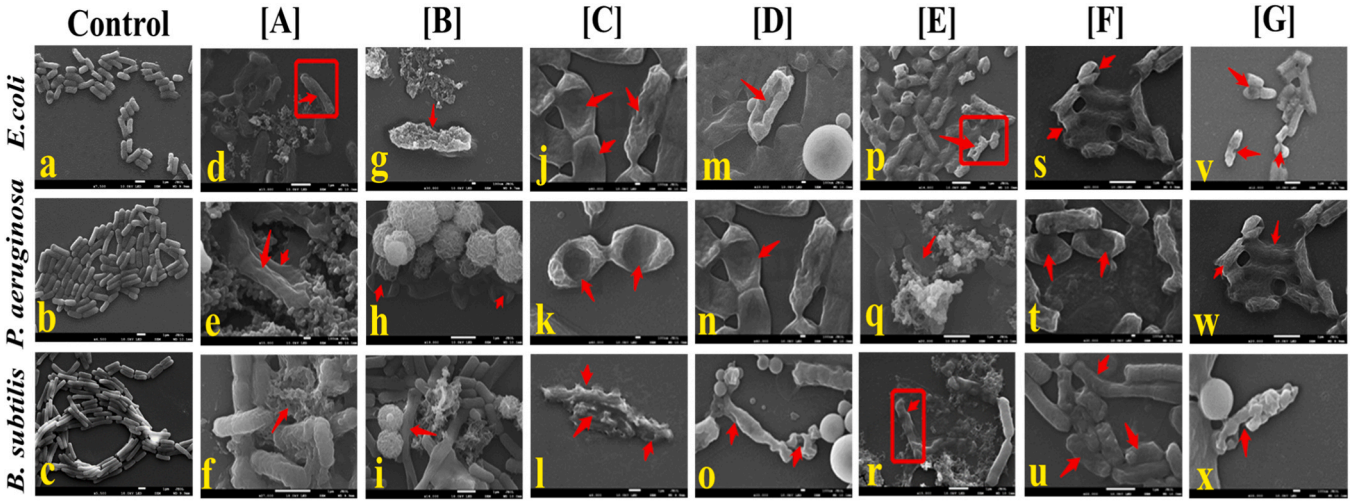

Fig. 6. SEM images displays the inhibition of targeted bacterial biofilms by α-Amp compounds. Images **(**a, b, and c) show untreated tested *bacterial* cells (controls). The antibacterial effect of the [A-G] compounds can be seen in (d-x) images. These images show the aggregation of mutated biofilms by α-Amp compounds and their binding with the bacterial cell. The cellular components are released when the bacterial cell wall breaks, as indicated by the red arrows.

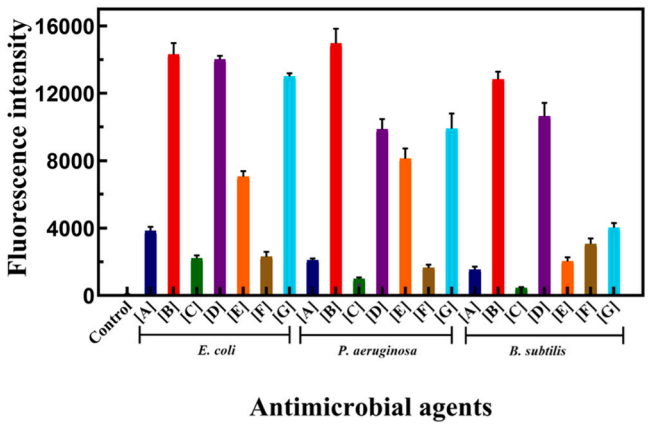

Fig. 7. Effect of the synthesized antibacterial agents on ROS generation.

α-Amp molecules. It has been reported that ROS disrupts the bacterial cell membrane and various cellular substances such as nucleic acids, proteins, and lipids [11,27]. Therefore, the application of ROS producing antibacterial compounds in water disinfection is promising in this field because of the low cost and ecologically beneficial features.

4.5. Elimination of the extracellular polymeric substance

Bacterial colonization does not just relate to the attachment of free bacteria to a particular surface; rather, it is primarily concerned with the production of structured aggregations of microorganisms and the extracellular polymeric matrix that are collectively referred to as biofilm. The extracellular polymeric substances of microbial biofilms give the biofilm cells structural stability as well as protection. In fact, one of the primary functions of extracellular proteins is to aid the first colonization procedures carried out by planktonic cells. In addition, EPS is made up of enzymes, which, among other things, allow for the digestion of exogenous macromolecules for the purpose of food acquisition and the breakdown of structural biofilm macromolecules in order to release free cells for new colonization processes. EPS includes lipids, proteins, carbohydrates, and nucleic acids [35]. Additionally, EPS hinder the accessibility of antibacterial agents to bacterial cells and inhibit their activity. Therefore, it is critical to design an effective antibacterial agent that can prevent or limit EPS formation.

In addition, the α-Amp compound [B] inhibited the protein of the EPS components of *E. coli*, *P. aeruginosa*, and *B. subtilis*. To prove this inhibition effect, the green fluorescence protein (GFP) was cloned into an expression plasmid and then transformed into the three bacterial strains. The expression of GFP under the effect of the α-Amp compound [B] was monitored using SDS-PAGE and fluorescence microscopy. The expression of GFP was progressively hindered by increasing the concentration of compound [B], ultimately resulting in total inhibition at the minimum inhibitory concentration (MIC) of 3.13 μg/mL, as depicted in Fig. 8**a**. The result attributes an excellent protein deterioration. Fig. 8**b** illustrates the variation in fluorescence intensity among the expressed recombinant GFPs. The GFP that was generated in the absence of exposure to compound [B] exhibited a high level of fluorescence intensity. In contrast, the fluorescence intensity exhibited an increase at lower minimum inhibitory concentration (MIC) values treated with [B], eventually approaching blank at the MIC value of 3.13 μg/mL for *E. coli* and *P. aeruginosa* cells. In a comparison, it is noted that the fluorescence intensity of *B. subtilis* demonstrates a similar declining pattern as the minimum inhibitory concentration (MIC) value rises, and it can entirely vanish upon reaching the experimental MIC value of 6.25 μg/mL.

The effect of α-Amp compounds against polysaccharides of targeted bacterial biofilms is displayed in Fig. 9. Fluorescein isothiocyanate (FTIC) specific dye was used to label the polysaccharide substances in the untreated (Fig. 9 **(a-c)**) and treated bacterial biofilms (Fig. 9 **(d-x)**) [56]. As shown in Fig. 9 **((g-i), (m-o), (p-r), (v-x))** for compounds **[**B], [D], [E], and [G], respectively, a low fluorescence color in the samples, demonstrating a high deformation effect against polysaccharide components in targeted bacteria when compared with the untreated bacteria. In addition, compound [A] (Fig. 9 **(d-f)**) consistently showed a high color intensity associated with a low reduction effect for the polysaccharide content, which revealed a weak uppermost eradication behavior compared with other treated and untreated bacterial cells. For compounds [C] (Fig. 9 **(j-i)**) and [F] (Fig. 9 **(s-u)**), a low eradication behavior against *E. coli* and *B. subtilis* biofilms is observed; however, for *P. aeruginosa*, these two α-Amp$_s$ showed high efficiency for polysaccharide reduction.

Following the same steps, bacterial cells were treated with a DAPI fluorescence stain to illustrate the effect of α-Amp analogues against nucleic acid of EPS [22], as shown in Fig. 10. The efficiency of α-Amp$_s$ against the nucleic acid of bacterial biofilms varied from one compound to another according to bacterial cell type. Compounds [B] and [G] showed (Fig. 10 **(g-i, v-x)**) the uppermost annihilation of nucleic acid compared to the untreated bacterial (Fig. 10 **(a-c)**). Besides, the compound [D] (Fig. 10 **(m-o)**) revealed better obliteration of the nucleic acid of *P. aeruginosa* and *B. subtilis* than *E. coli* biofilms. Similarly, compound [E] (Fig. 10 **(p-r)**) shows better reduction efficiency for nucleic acid against *P. aeruginosa* and *B. subtilis*; however, it does not show effective annihilation of the nucleic acid of *E. coli (*quite similar to the untreated

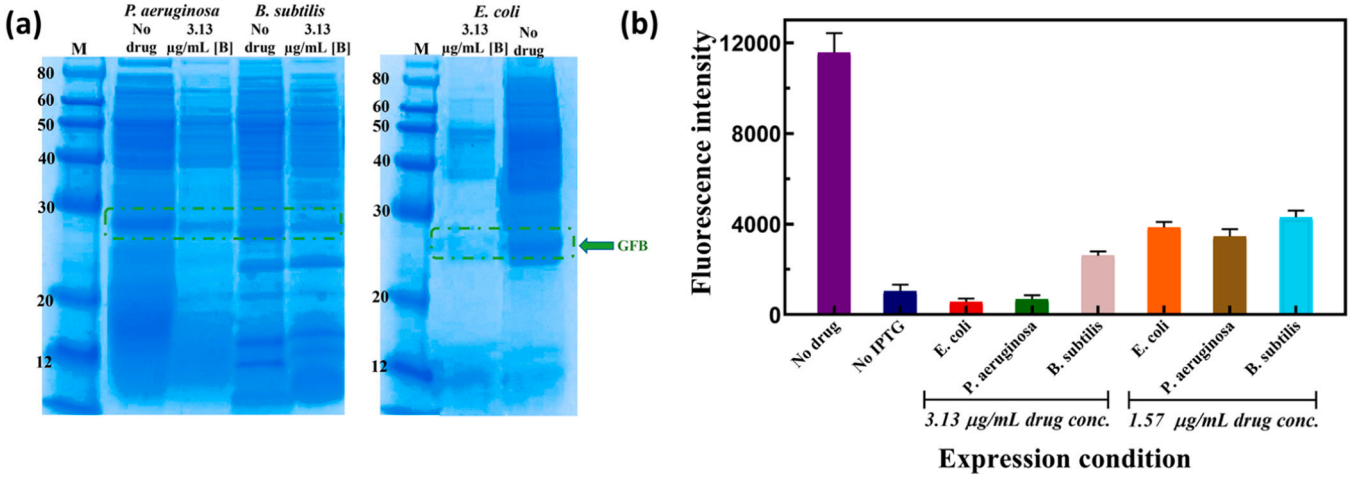

Fig. 8. Inhibition of recombinant GFP expression in tested cells after treatment with compound [B]. (a) SDS-PAGE and (b) GFP fluorescence intensity of the soluble proteins produced by tested cells in the presence or absence of compound [B].

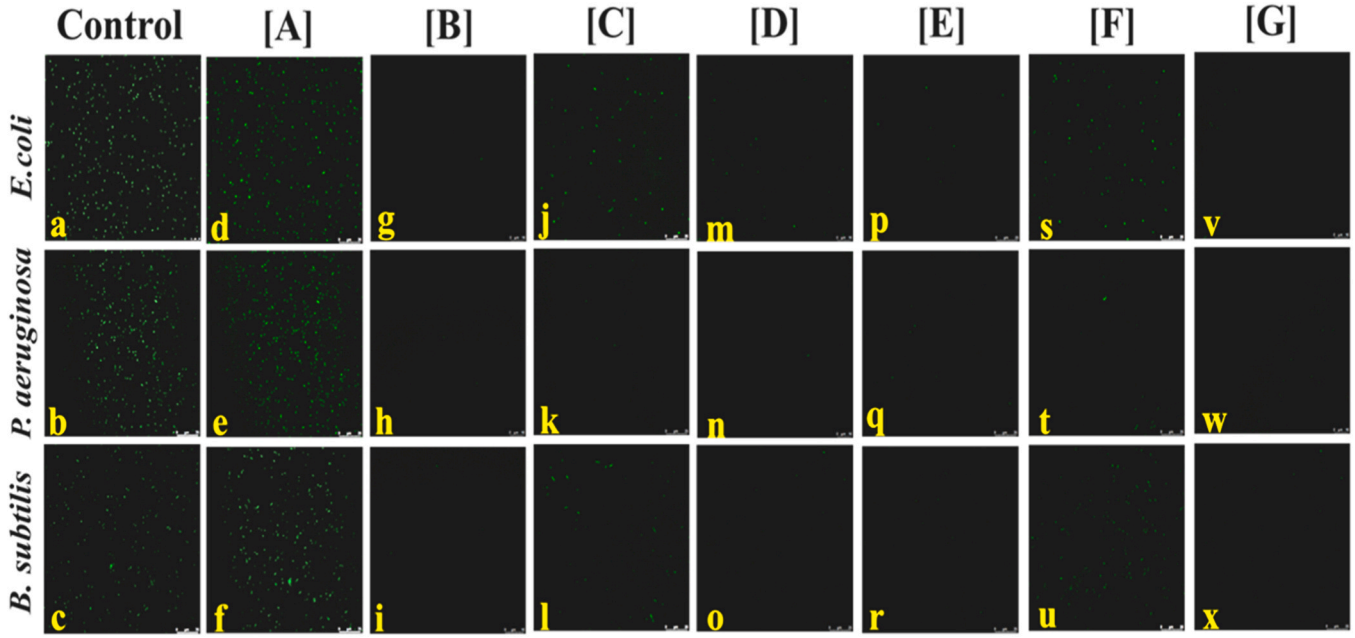

Fig. 9. Confocal fluorescence images of targeted bacterial biofilms' polysaccharide stained with FITC (fluorescein isothiocyanate) at 495/519 nm (excitation/ emission wavelengths). Images a-c show the untreated biofilms (controls) and d-x report the treated biofilms with α-Amp analogues.

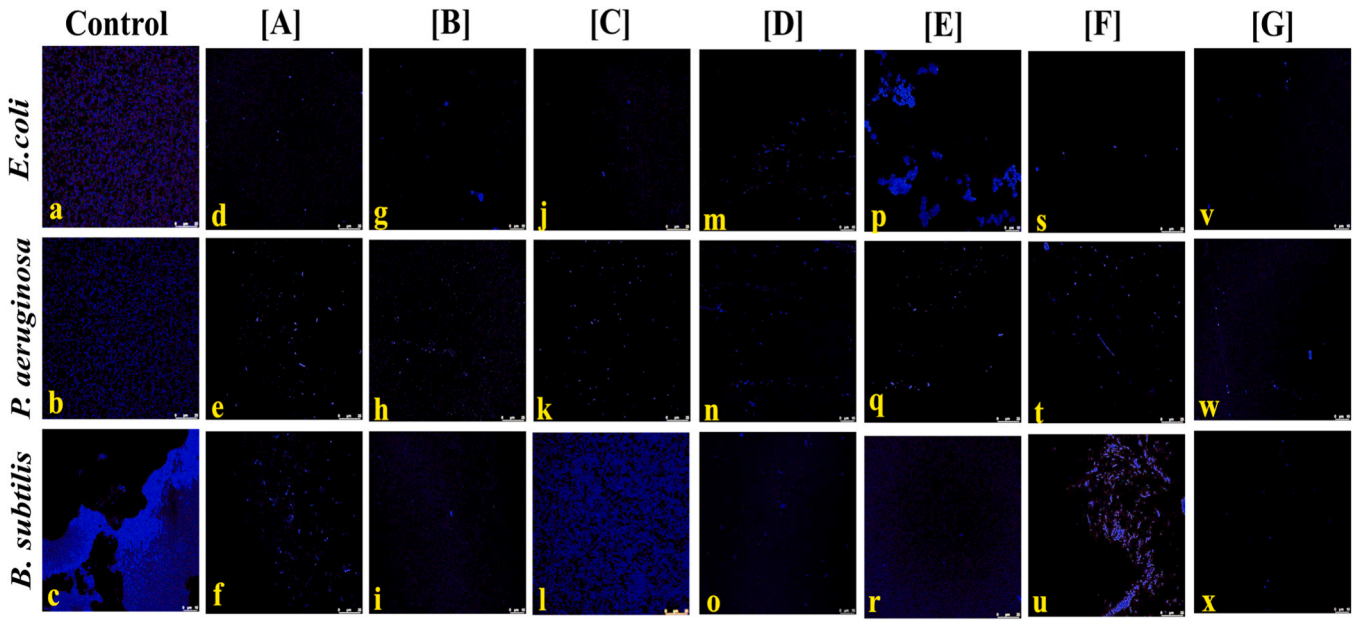

Fig. 10. Confocal fluorescence images of targeted bacterial biofilms' nucleic acid stained with DAPI at 358/461 nm for excitation/ emission wavelengths. Images a-c indicate the untreated biofilms (controls) and d-x indicate those treated with α-Amp analogues.

E. coli biofilm). Nonetheless, the other α-Amp compounds display different competencies, such as compounds [A] (Fig. 10 **(d-f)**), [C] (Fig. 10 **(j-i)**) and [F] (Fig. 10 **(s-u)**), which showed a better efficiency against nucleic acid of *P. aeruginosa* and *E. coli* biofilms than *B. subtilis* biofilm, suggesting low effectiveness toward nucleic acid of gram-positive bacteria (i.e., *B. subtilis*).

The process of biofilm formation was observed by utilizing the Film Tracer, SYPRO Ruby biofilm matrix stain, that is a typical method to expose various protein types including lipoproteins, glycoproteins, calcium-binding proteins, phosphoproteins, fibrillar and other kinds of proteins [66]. The existence of these protein complexes confers structural integrity to biofilms. Fig. 11 **(a-c)** depict the biofilm formation of untreated cells for each targeted bacteria, whereas Fig. 11 **(d-x)** illustrate the inhibitory impact resulting from the presence of α-Amp analogues, as indicated by the application of a particular dye. The findings demonstrated a significant inhibitory effect on the EPS protein complex in specific bacteria by α-Amp analogues, particularly compounds [B] to [G]. Simultaneously, chemical [A] exhibits a weak inhibitory impact on the EPS protein complex of the bacterial strains under investigation, particularly in the case of *B. subtilis*.

The eradication of bacterial biofilms using α-Amp analogues was further confirmed using SYTO 9 and propidium iodide dye, as shown in Fig. 12. Notably, in Fig. 12, the live cells appear green colored (due to Syto9 stain), while the dead cells visualized as red colored (revealed by

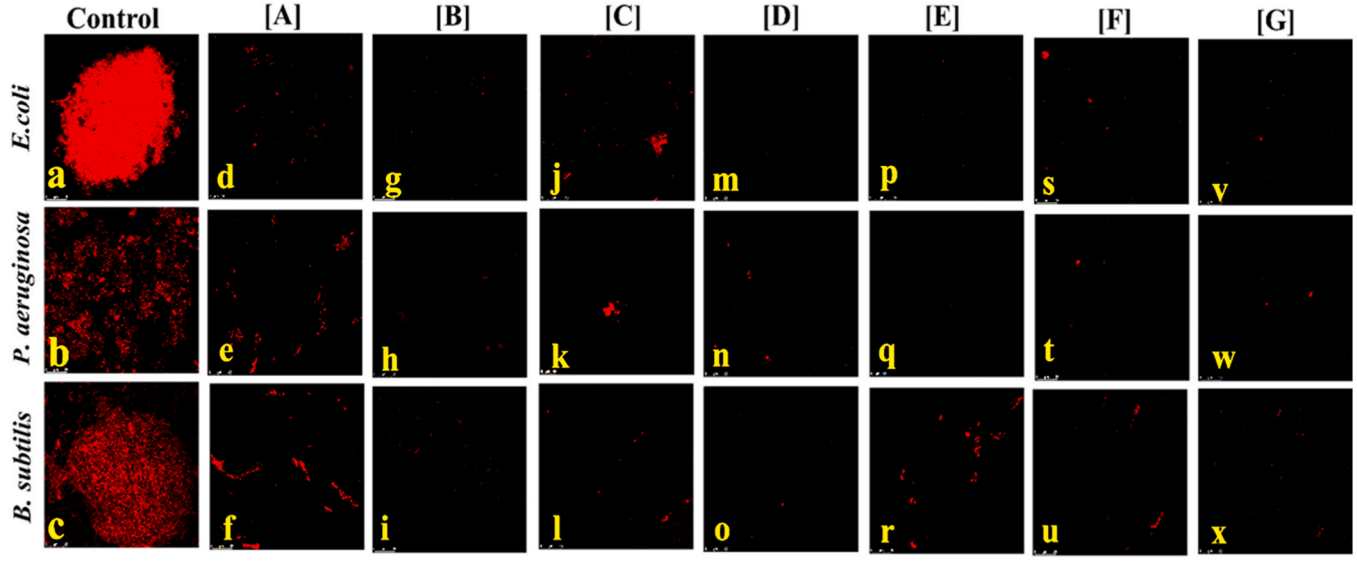

Fig. 11. Confocal fluorescence images of represented bacteria biofilms' protein stained with SYPRO Ruby biofilm matrix at excitation/ emission wavelengths of 450/ 610 nm. Images **a-c** show the untreated biofilms and **d-x** reported biofilms with α-Amp analogues.

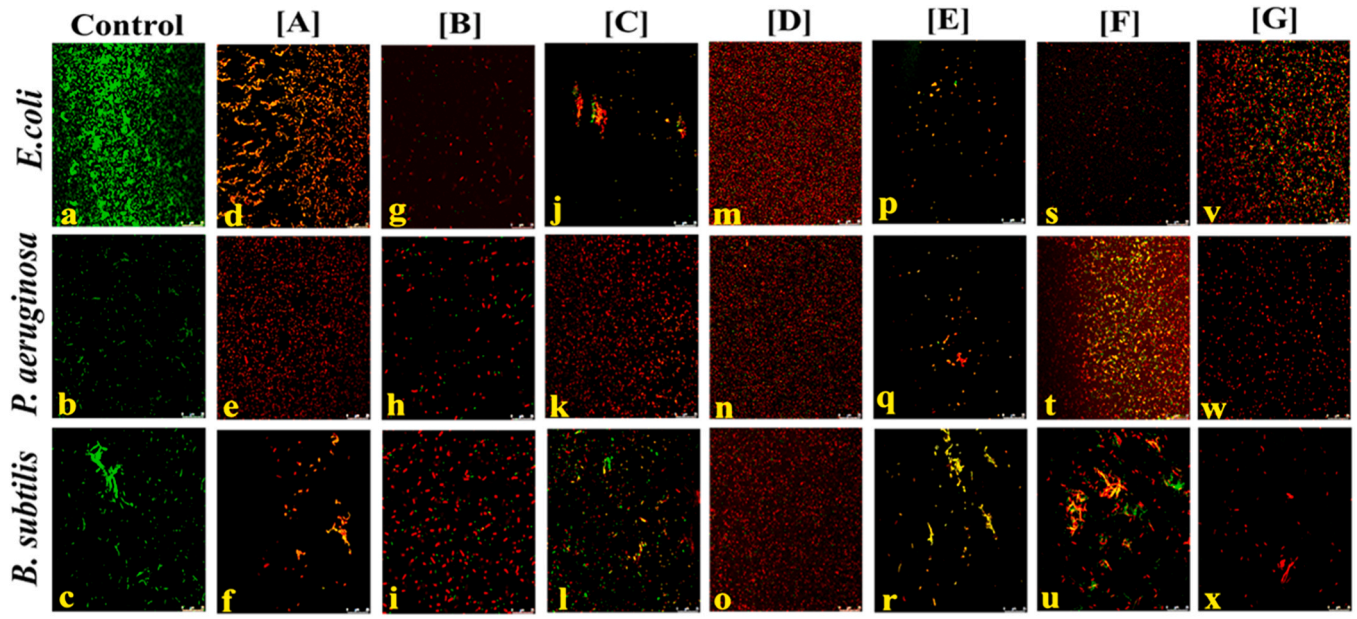

Fig. 12. Confocal fluorescence micrographs of represented bacteria biofilms stained with live cells (green: Syto 9) and dead cells (red: propidium iodide). Images **a-c** show the untreated biofilms (controls) and **d-x** report the biofilms treated with α-Amp analogues.

propidium iodine dye). Fig. 12 **(a-c)** shows the untreated bacterial biofilms with a noticeable green spectrum, suggesting a high population of live bacterial cells. In contrast, upon treatment of the bacterial biofilms with the antibiotic chemicals, a predominant population of deceased cells exhibiting a red color was observed, accompanied by a minimal presence of live cells displaying a faint green coloration. This observation provides confirmation that α-Amp analogues exhibit a significant reduction in the viability of biofilms. In detail, among α-Amp analogues, compounds [B], [D], and [G] show an effective annihilation performance with a high population of the dead cell (red colored) against all tested bacterial biofilms viability (Fig. 12 **(g-i, m-o, v-x)**). Additionally, compound [A] (Fig. 12 **(d-f)**), compound [C] (Fig. 12 **(j-l)**), and compound [F] (Fig. 12 **(s-u)**) also reveal the same reducing action against bacterial biofilms, but with a lesser eradication activity on the biofilms in comparison with compounds [B], [D], and [G]. However, compound [E] (Fig. 12 **(p-r)**) shows a mishmash of dead and live cells, demonstrating the partial reduction of tested bacterial biofilms.

5. Molecular docking study

To bestow substances with strong antibacterial activity, it is imperative that they have a strong affinity and favourable interactions with certain bacterial proteins, consequently hindering normal metabolic processes. As a result, the primary objective of molecular docking studies is to investigate the plausibility of this binding process and provide insights into the specific interactions that may contribute to the efficacy of these molecules as potential therapeutic agents. The aforementioned notion serves as the fundamental basis for the field of structure-based medication design [6]. Molecular docking study were applied on α-Amp analogues to: (a) investigate their affinity for gram

positive and gram-negative bacteria proteins (PDB: 2FQT ⁋and 6YD9⁋), and (b) predict their eligibility as antibacterial agents in a step to explore their target protein in addition to the biological investigation. The outcomes of docking α-Amp analogues in all the downloaded proteins showed the chemical bonding type with the amino acids engaged in the protein interaction. Table S3 summarizes the values recorded for binding affinity and root mean square deviation (RMSD). The binding affinity data reveals that the seven synthesized compounds exhibit varying binding capacities with the three selected bacterial proteins, suggesting a pronounced attraction between these compounds and the proteins which potentially disrupts the bacterial mechanisms, underpinning their antibacterial activity. It has been observed that the compound [B] has minimum binding energy of − 6.650 kCal/mol and the compound [E] has a maximum of − 5.363 kCal/mol for protein 2FQT, whereas in the case of *E. coli* the minimum binding energy was obtained for compound [A] (− 8.70 kCal/mol) and the maximum for the compound [G] (− 4.41 kCal/mol). Similarly, based on the lowest MIC obtained compounds (B, D, and G), the binding energy of *P. aerugiosa* bacterial was calculated with protein 3HEM, and the minimum binding energy has been observed for compound [D] with the value of − 8.027 kCal/mol, but compound [B] and [G] shows binding energies of − 6.169 and − 6.214 kCal/mol, respectively. The difference between the maximum and minimum value of the binding energies in all cases is rather low, indicating that all the compounds have good activity toward selected bacterial proteins. The calculation of Glide Ligand Efficiency is crucial in molecular docking as it provides insights into the ligand's binding strength relative to its size. This metric helps in the identification of ligands that achieve strong binding while maintaining minimal molecular weight. It aids in the selection of ligands with optimal pharmacological properties for further drug development. These calculations are crucial because they provide insights into the efficiency of ligands in binding to the protein target. Higher ligand efficiency values indicate that the ligand is more efficient in achieving strong binding while minimizing its molecular weight, which is desirable for designing new drugs. Variations in ligand efficiency and embedded energy values among ligands and proteins docking observed infer that the ligands have strong interactions with proteins, which can identify the most favorable interactions with specific proteins. There are different types of interactions including H-bonding and hydrophobic H-*pi* interactions with the binding sites of all the investigated proteins as shown in Table S3. Despite the absence of significant hydrogen bonds in the majority of docking results, the noteworthy findings from the analysis of binding affinity indicate the prevalence of multiple weak van der Waals interactions, as well as pi and sigma-related interactions within the docked complexes. These interactions contribute to the formation of stable conformations between the proteins and compounds, underscoring their potential for robust antibacterial activity, as corroborated by experimental data.

It has been observed that the compound [B] has prominent experimental antibacterial activities therefore the interactions of this compound with studied proteins have been illustrated thoroughly to investigate its theoretical antibacterial potency. The bindings of compound [B] at the site of interaction in both lyase protein from *bacillus* and DNA gyrase for *E. coli* are illustrated in Fig. 13 **(a-b)** and Fig. S4 **(a-d)** whereas no interaction has been observed in the case of the third protein (i.e., 3HEM with the compound [B]). The key interactions in the docked complexes uncovered that the majority of the interlinkages have been accomplished through the electronegative atoms and the *pi*-cloud of the compound mainly with the polar amino acid residues (Asp, Glu, His, Arg, and Asn) and in very few cases, the non-polar residues like Pro, Met, Ile, and Gly have also been involved. In both cases, compound [B] has a greater number of strong interactions, mainly of H-donor, H-acceptor, and *pi*-H with the varieties of the amino acid residues which further intensify the potent activeness of this compound towards both types of bacterial strains.

In terms of binding affinity, compound [B] recorded a strong association with two proteins with a binding affinity of − 6.650 for the lyase protein of gram-positive bacteria (*B. subtilis*) and − 6.461 for DNA gyrase of Gram-negative bacteria (*E. coli*). The interactions observed for compound [B] include two H-donor with Glu57 and Asp78 residue, one pi-H with His54 residue, and one cation-pi with His58 residue of 2FQT protein of *B. subtilis* whereas one H-donor with Asp49 residue, one H-acceptor with Arg136 residue, and one *pi*-H with Pro79 residue of the 6YD9 protein structure of *E. coli*. Besides compound [B], compound [A] is the next one with the best potential in terms of both binding energy and the interactions present. The experimental results and the observed docking results are in agreement, suggesting that theoretical

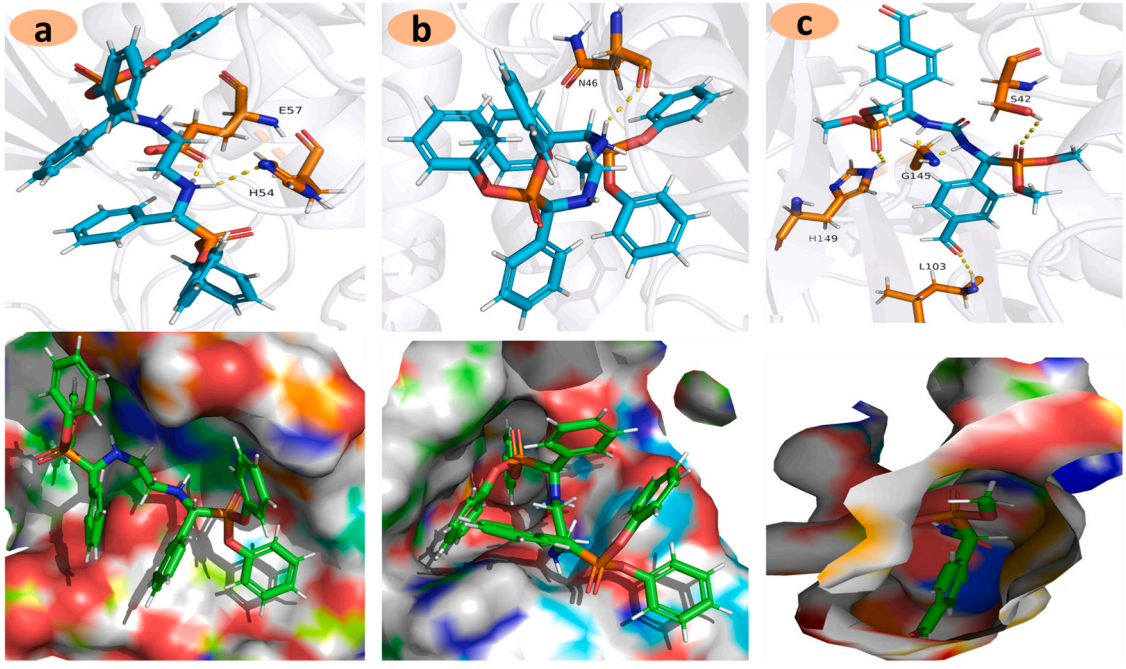

Fig. 13. Site view and surface of interaction showing compound [B] in orange complexed with the co-crystalized ligand in (a) cyan ball and stick in protein 2FQT (b) green stick in protein 6YD9 and (c) protein 3HEM.

computation is required in addition to the experimental analysis [1,3]. From the analysis of both the calculated binding energies and observed interactions present between the ligands and receptor, it can be inferred that the compounds having a greater number of aromatic rings and the electronegative atoms have stronger activity towards the bacterial protein. The docking analyses of the compounds with the co-crystallized ligands utilized as a reference for the active site have also demonstrated that the as-synthesized compounds have a high binding affinity toward the receptor proteins' active; this contributes to the validation of the identification of docking sites on the receptor systems of potent compounds [1].

Previously, it was believed that organophosphorus-based frame compounds showed an excellent approach toward mammalian cells owing to their high biological activity [2,43,50,67,9]; that is why a class of α-aminophosphonate was gradually researched and considered a unique antibacterial drug for antibacterial activity. With this inspiration, α-aminophosphonate-derived compounds were prepared in this study and are believed to be effective as antibacterial material. All prepared compounds revealed outstanding therapeutic results associated with N-heterocyclic synchronized combinations in their atomic structure, which contribute to the destruction of cell membrane walls. Thus, compound [B] showed a broad scope of antibacterial activities.

The unique properties of α-aminophosphonate compounds promote electrostatic binding with the negative and positive surfaces of tested bacteria, improving interaction with the phospholipid membrane (as illustrated in Scheme 2) [11]. Because of this, the formation of a polar tail supports the variation between the membrane-water interfaces and increases the permeability, and the fatal effect is strengthened (as confirmed by SEM images). This can make a leakage path in the membrane for the bacterial cell after the incorporation of the peptide. In addition, the fatal effect is strengthened. In addition to this, the presence of the organophosphorus species may hinder bacterial cells from maturing and create water molecule permeability, both of which may set off an oxidative stress reaction and, ultimately, result in the extinction of the bacteria [24,64]. The basal planes of α-Amp$_s$ may be trapped in the bacterial cell due to a π–π bond interaction with the amide groups present in the cell walls of the bacteria. Besides, the carbon-free radicals arise on the bacterial surface, which could also help to damage the cell wall and generate ROS [40]. Therefore, these α-Amp analogues revealed a significant effect on breaking the bacterial cell membrane, nucleic acid, and polysaccharides (as discussed in Figs. 6, 7, and 8).

The antibacterial mechanism of α-aminophosphonate compounds generally work according to these three models:

1. Wormhole formation by covering the bacterial membrane to its saturation point: Cross-enlargements in the polar head group cause the lipid to bend, and antibacterial α-Amp fill the voids [15].
2. Ions and chemicals can cross the bacterial membrane owing to the adhered phospholipid head groups [59].
3. Amphipathic transmembrane holes could be formed due to electrostatic contact with the outside of the cell membrane [15].

A schematic scheme was displayed (Scheme 2) to demonstrate the antibacterial mechanism of α-Amp$_s$, showing ROS generation, membrane destruction, and EPS component reduction.

6. Conclusions

A green approach was used to prepare different α-Amp analogues with different amines and aldehydes using ionic liquid as a catalyst and solvent. FT-IR, and ^{1}H, ^{13}C, ^{31}P NMR were used to confirm the synthesis of organophosphorus compounds. The combination of benzaldehyde (as aldehyde), with ethylenediamine monohydrate (as amine) and triphenyl phosphite (for compound [B]), delivered the best overall antibacterial performance against *E. coli*, *P. aeruginosa,* and *B. Subtilis*, at least compared with the other drugs (i.e., [A], [C], [D], [E], [F], and [G]) but also against two commercial antibacterial agents (i.e., kanamycin and streptomycin). Compound [B] significantly inhibited the bacterial growth with a maximum diameter of inhibition zone reached 41 mm for *E. coli*, 39 mm for *P. aeruginosa*, and 28 mm for *B. subtilis*. In addition, compound [B] shows MIC value as low as 3.13 μg/mL for *E. coli*, 3.13 μg/mL for *P. aeruginosa,* and 6.25 μg/mL for *B. subtilis*. Moreover, compound [B] significantly eradicated the mature biofilm of *E. coli*, *P. aeruginosa,* and *B. subtilis* at a concentration of 12.5, 12.5, and 25 μg/mL, respectively. SEM analysis of microorganisms confirmed the lethal effect of compound [B]. Elimination of the extracellular polymeric substances including polysaccharides, nucleic acid, and protein contributes to the outstanding antibacterial effect of compound [B].

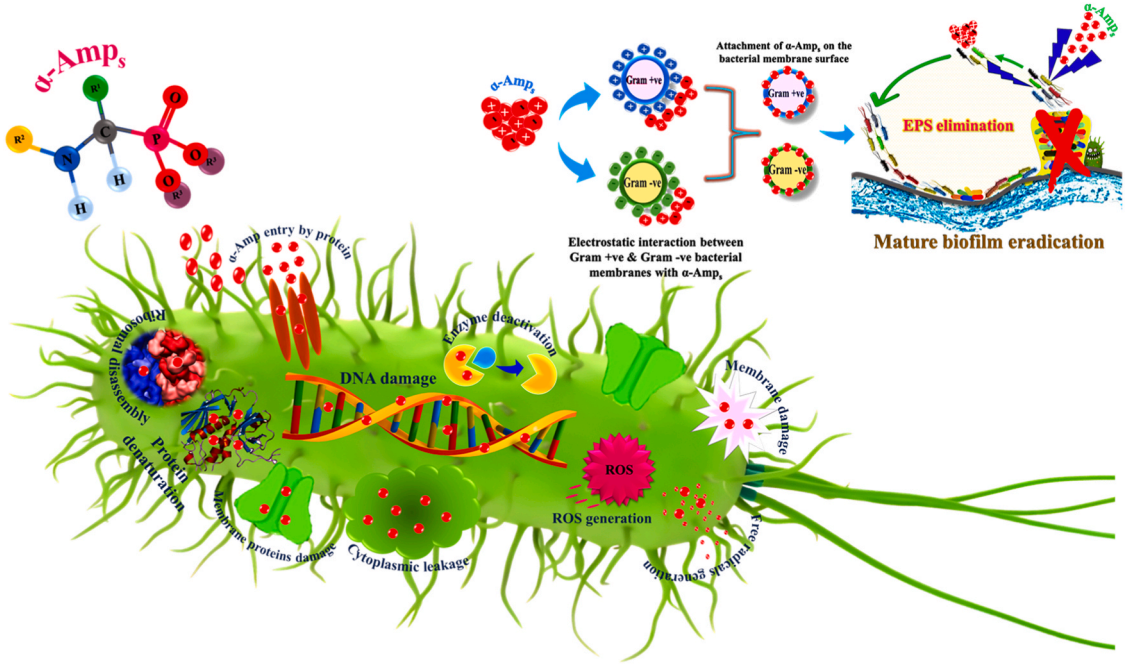

Scheme 2. Schematic diagram showing the predicted antibacterial mechanism of α-Amp analogues.

Interestingly, the docking study confirmed that compound [B] is the best among the other antibacterial agents due to its strong interactions with protein structures. This is shown by the values of binding affinity for the lyase protein of gram-positive bacteria *B. subtilis* (i.e., − 6.650 kCal/mol), and for DNA gyrase of gram-negative bacteria *E. coli* (i.e., − 6.461 kCal/mol).

The synthesis of the α-Amp analogues is unique, and they constitute a prospective, easy synthesis, low-cost, and safe antibacterial option for removing bacterial biofilms in water pipelines.

Environmental implication

The green one-pot method was carried out to synthesize different analogues of the environmentally friendly α-aminophosphonates as antibacterial agents for hazardous bacterial biofilm eradication. The resulting compounds showed significant antibacterial and antibiofilm activities with promising minimum inhibitory concentration values and efficient effects for the eradication of extracellular polymeric substances. Additionally, a novel mechanism for their antibacterial activity was proposed based on a comprehensive analysis of their antibacterial phenomena supported by theoretical modeling. This study introduced the development of antibacterial compounds for industrial purposes, particularly for cleaning water pipelines for domestic consumption and in achieving clean-water goals possibility.

CRediT authorship contribution statement

Rana R. Neiber: Methodology, Investigation, Formal analysis, Data curation, Writing-original draft. **Jianmin Xing and Jiayu Xin**: Conceptualization, Validation, Writing – review & editing. **Nadia A. Samak**: Supervision, conceptualization, biological experiments design and supervision, formal analysis, writing, reviewing, and editing. **Elshaymaa I. Elmongy**: Docking and software, Data curation. **Ahmed A. Galhoum and Ibrahim El-Tantawy El Sayed, Eric Guibal**: Conceptualization, Supervision, Materials Characterization, Visualization, Data curation, Writing – review & editing. **Xingmei Lu**: Supervision, Conceptualization, Resources, Funding, Investigation, Reviewing, Writing – review editing. All authors have read and agreed to the published version of the manuscript.

Declaration of Competing Interest

The authors declare that they have no known competing financial interests or personal relationships that could have appeared to influence the work reported in this paper.

Data availability

The authors do not have permission to share data.

Acknowledgments

This work was financially Supported by the National Key Research and Development Program of China (No. 2022YFB420180), the National Natural Scientific Fund of China (Nos. 22238011, 22178343, 22178358), International Partnership Program of Chinese Academy of Sciences (No. 2023VMA0001), the Key R & D projects in Hunan Province (No. 2021SK2047), the Strategic Priority Research Program of Chinese Academy of Science (Nos. XDA24030504, XDA29040700. The Alliance of International Science Organizations (ANSO) fellowship is also gratefully acknowledged for funding the Ph.D. project of Rana R. Neiber. Sincerely appreciate Prof. Suojiang Zhang (IPE, CAS) for his careful academic guidance and great support.

Appendix A. Supporting information

Supplementary data associated with this article can be found in the online version at doi:10.1016/j.jhazmat.2023.133203.

References

[1] Abd El-Karim, S.S., Mohamed, H.S., Abdelhameed, M.F., Amr, A.E.-G.E., Almehizia, A.A., Nossier, E.S., 2021. Design, synthesis and molecular docking of new pyrazole-thiazolidinones as potent anti-inflammatory and analgesic agents with TNF-α inhibitory activity. Bioorg Chem 111, 104827. https://doi.org/10.1016/j.bioorg.2021.104827.

[2] Ahmed, A.A.S., Awad, H.M., El-Sayed, I.E.-T., El Gokha, A.A., 2020. Synthesis and antiproliferative activity of new hybrids bearing neocryptolepine, acridine and α-aminophosphonate scaffolds. J Iran Chem Soc 17, 1211–1221. https://doi.org/10.1007/s13738-019-01849-2.

[3] Akkoc, S., Karatas, H., Muhammed, M.T., Kökbudak, Z., Ceylan, A., Almalki, F., et al., 2022. Drug design of new therapeutic agents: molecular docking, molecular dynamics simulation, DFT and POM analyses of new Schiff base ligands and impact of substituents on bioactivity of their potential antifungal pharmacophore site. J Biomol Struct Dyn 1–14. https://doi.org/10.1080/07391102.2022.2111360.

[4] Andrea, A., Molchanova, N., Jenssen, H., 2018. Antibiofilm peptides and peptidomimetics with focus on surface immobilization. Biomolecules 8, 27. https://doi.org/10.3390/biom8020027.

[5] Ayukekbong, J.A., Ntemgwa, M., Atabe, A.N., 2017. The threat of antimicrobial resistance in developing countries: causes and control strategies. Antimicrob Resist Infect Control 6, 47. https://doi.org/10.1186/s13756-017-0208-x.

[6] Belal, A., Abdel Gawad, N.M., Mehany, A.B.M., Abourehab, M.A.S., Elkady, H., Al-Karmalawy, A.A., et al., 2022. Design, synthesis and molecular docking of new fused 1 *H*-pyrroles, pyrrolo [3, 2-*d*] pyrimidines and pyrrolo [3, 2-*e*][1,4] diazepine derivatives as potent EGFR/CDK2 inhibitors. J Enzym Inhib Med Chem 37, 1884–1902. https://doi.org/10.1080/14756366.2022.2096019.

[7] Beloin, C., Renard, S., Ghigo, J.-M., Lebeaux, D., 2014. Novel approaches to combat bacterial biofilms. Curr Opin Pharmacol 18, 61–68. https://doi.org/10.1016/j.coph.2014.09.005.

[8] Bi, Y., Xia, G., Shi, C., Wan, J., Liu, L., Chen, Y., et al., 2021. Therapeutic strategies against bacterial biofilms. Fundam Res 1, 193–212. https://doi.org/10.1016/j.fmre.2021.02.003.

[9] Boshta, N.M., Elgamal, E.A., El-Sayed, I.E.T., 2018. Bioactive amide and α-aminophosphonate inhibitors for methicillin-resistant *Staphylococcus aureus* (MRSA). Mon Chem 149, 2349–2358. https://doi.org/10.1007/s00706-018-2303-y.

[10] Budič, M., Rijavec, M., Petkovšek, Z., Zgur-Bertok, D., 2011. *Escherichia coli* bacteriocins: antimicrobial efficacy and prevalence among isolates from patients with bacteraemia. PLoS One 6, e28769. https://doi.org/10.1371/journal.pone.0028769.

[11] Chan, D.I., Prenner, E.J., Vogel, H.J., 2006. Tryptophan- and arginine-rich antimicrobial peptides: structures and mechanisms of action. Biochim Et Biophys Acta (BBA) - Biomembr 1758, 1184–1202. https://doi.org/10.1016/j.bbamem.2006.04.006.

[12] Cherenok, S., Vovk, A., Muravyova, I., Shivanyuk, A., Kukhar, V., Lipkowski, J., et al., 2006. Calix[4]arene α-Aminophosphonic acids: asymmetric synthesis and enantioselective inhibition of an alkaline phosphatase. Org Lett 8, 549–552. https://doi.org/10.1021/ol052469a.

[13] Choi, K.-H., Kumar, A., Schweizer, H.P., 2006. A 10-min method for preparation of highly electrocompetent *pseudomonas aeruginosa* cells: application for DNA fragment transfer between chromosomes and plasmid transformation. J Microbiol Methods 64, 391–397. https://doi.org/10.1016/j.mimet.2005.06.001.

[14] Chu, L., Wang, J., He, S., Chen, C., Wojnárovits, L., Takács, E., 2021. Treatment of pharmaceutical wastewater by ionizing radiation: Removal of antibiotics, antimicrobial resistance genes and antimicrobial activity. J Hazard Mater 415, 125724. https://doi.org/10.1016/j.jhazmat.2021.125724.

[15] Costa, F., Carvalho, I.F., Montelaro, R.C., Gomes, P., Martins, M.C.L., 2011. Covalent immobilization of antimicrobial peptides (AMPs) onto biomaterial surfaces. Acta Biomater 7, 1431–1440. https://doi.org/10.1016/j.actbio.2010.11.005.

[16] Costerton, J.W., Stewart, P.S., Greenberg, E.P., 1999. Bacterial biofilms: a common cause of persistent infections. Sci 284, 1318–1322. https://doi.org/10.1126/science.284.5418.1318.

[17] Deng, Z., Sun, H., Bheemanaboina, R.R.Y., Luo, Y., Zhou, C.-H., 2022. Natural aloe emodin-hybridized sulfonamide aminophosphates as novel potential membrane-perturbing and DNA-intercalating agents against *Enterococcus faecalis*. Bioorg Med Chem Lett 64, 128695. https://doi.org/10.1016/j.bmcl.2022.128695.

[18] Elmongy, E.I., Altwaijry, N., Attallah, N.G.M., AlKahtani, M.M., Henidi, H.A., 2022. In-silico screening of novel synthesized thienopyrimidines targeting Fms related receptor tyrosine kinase-3 and their In-Vitro biological evaluation. Pharmaceuticals 15, 170. https://doi.org/10.3390/ph15020170.

[19] Elmongy, E.I., Henidi, H.A., 2022. In silico evaluation of a promising key intermediate thieno [2, 3-d] pyrimidine derivative with expected JAK2 kinase inhibitory activity. Molbank 2022, M1352. https://doi.org/10.3390/M1352.

[20] Elsherbiny, D.A., Abdelgawad, A.M., El-Naggar, M.E., El-Sherbiny, R.A., El-Rafie, M.H., El-Sayed, I.E.-T., 2020. Synthesis, antimicrobial activity, and sustainable release of novel α-aminophosphonate derivatives loaded carrageenan

cryogel. Int J Biol Macromol 163, 96–107. https://doi.org/10.1016/j.ijbiomac.2020.06.251.
[21] Erturk, Ö., Kati, Hatice, Yayli, Nurettin, Demirbag, Z., 2003. Antimicrobial activity of Viscum album L. subsp. abietis (Wiesb). Turk J Biol 27, 255–258. ⟨https://journals.tubitak.gov.tr/biology/vol27/iss4/9⟩.
[22] Estandarte, A.K., Botchway, S., Lynch, C., Yusuf, M., Robinson, I., 2016. The use of DAPI fluorescence lifetime imaging for investigating chromatin condensation in human chromosomes. Sci Rep 6, 31417. https://doi.org/10.1038/srep31417.
[23] Ewies, E.F., El-Hussieny, M., El-Sayed, N.F., Fouad, M.A., 2019. Design, synthesis and biological evaluation of novel α-aminophosphonate oxadiazoles via optimized iron triflate catalyzed reaction as apoptotic inducers. Eur J Med Chem 180, 310–320. https://doi.org/10.1016/j.ejmech.2019.07.029.
[24] Fatthallah, N.A., Selim, M.S., El Safty, S.A., Selim, M.M., Shenashen, M.A., 2021. Engineering nanoscale hierarchical morphologies and geometrical shapes for microbial inactivation in aqueous solution. Mater Sci Eng: C 122, 111844. https://doi.org/10.1016/j.msec.2020.111844.
[25] Friedman, M., Henika, P.R., Mandrell, R.E., 2003. Antibacterial activities of phenolic benzaldehydes and benzoic acids against *Campylobacter jejuni*, *Escherichia coli*, *Listeria monocytogenes*, and *Salmonella enterica*. J Food Prot 66, 1811–1821. https://doi.org/10.4315/0362-028X-66.10.1811.
[26] Gao, Y.-R., Cao, J.-F., Shu, Y., Wang, J.-H., 2021. Research progress of ionic liquids-based gels in energy storage, sensors and antibacterial. Green Chem Eng 2, 368–383. https://doi.org/10.1016/j.gce.2021.07.012.
[27] Guo, Q., Luo, Y., Guo, H., Lan, T., Wang, S., Geng, K., et al., 2022. A photo-thermal nanocomposite capable of relieving inflammatory response to compete multidrug-resistant *pseudomonas aeruginosa* infection. Chem Eng J 446, 137173. https://doi.org/10.1016/j.cej.2022.137173.
[28] Habiba, K., Bracho-Rincon, D.P., Gonzalez-Feliciano, J.A., Villalobos-Santos, J.C., Makarov, V.I., Ortiz, D., et al., 2015. Synergistic antibacterial activity of PEGylated silver–graphene quantum dots nanocomposites. Appl Mater Today 1, 80–87. https://doi.org/10.1016/j.apmt.2015.10.001.
[29] Hardalo, C., Edberg, S.C., 1997. *Pseudomonas aeruginosa*: Assessment of risk from drinking water. Crit Rev Microbiol 23, 47–75. https://doi.org/10.3109/10408419709115130.
[30] Hetrick, E.M., Schoenfisch, M.H., 2006. Reducing implant-related infections: active release strategies. Chem Soc Rev 35, 780–789. https://doi.org/10.1039/B515219B.
[31] Imam, E.A., El-Tantawy El-Sayed, I., Mahfouz, M.G., Tolba, A.A., Akashi, T., Galhoum, A.A., et al., 2018. Synthesis of α-aminophosphonate functionalized chitosan sorbents: effect of methyl vs phenyl group on uranium sorption. Chem Eng J 352, 1022–1034. https://doi.org/10.1016/j.cej.2018.06.003.
[32] Inc C.C.G., 2014. Molecular Operating Environment (MOE), Montreal, QC, Canada. ⟨https://www.chemcomp.com/Products.htm⟩.
[33] Kiefer, R., Höll, W.H., 2001. Sorption of heavy metals onto selective ion-exchange resins with aminophosphonate functional groups. Ind Eng Chem Res 40, 4570–4576. https://doi.org/10.1021/ie010182l.
[34] Kraicheva, I., Bogomilova, A., Tsacheva, I., Momekov, G., Troev, K., 2009. Synthesis, NMR characterization and in vitro antitumor evaluation of new aminophosphonic acid diesters. Eur J Med Chem 44, 3363–3367. https://doi.org/10.1016/j.ejmech.2009.03.017.
[35] Lee, J.-K., Mereuta, L., Luchian, T., Park, Y., 2019. Antimicrobial peptide HPA3NT3-A2 effectively inhibits biofilm formation in mice infected with drug-resistant bacteria. Biomater Sci 7, 5068–5083. https://doi.org/10.1039/C9BM01051C.
[36] Li, Y., Parry, G., Chen, L., Callahan, J.A., Shaw, D.E., Meehan, E.J., et al., 2007. An anti-urokinase plasminogen activator receptor (uPAR) antibody: crystal structure and binding epitope. J Mol Biol 365, 1117–1129. https://doi.org/10.1016/j.jmb.2006.10.059.
[37] Lister, P.D., Wolter, D.J., Hanson, N.D., 2009. Antibacterial-resistant Pseudomonas aeruginosa: clinical impact and complex regulation of chromosomally encoded resistance mechanisms. Clin Microbiol Rev 22, 582–610. https://doi.org/10.1128/cmr.00040-09.
[38] Ma, H., Zhang, L., Huang, X., Ding, W., Jin, H., Li, Z., et al., 2019. A novel three-dimensional galvanic cell enhanced Fe^{2+}/persulfate system: high efficiency, mechanism and damaging effect of antibiotic resistant *E. coli* and genes. Chem Eng J 362, 667–678. https://doi.org/10.1016/j.cej.2019.01.042.
[39] Mahmoud, M.E., Adel, S.E., El-Sayed, I.E.T., 2020. Development of titanium oxide-bound-α-aminophosphonate nanocomposite for adsorptive removal of lead and copper from aqueous solution. Water Resour Ind 23, 100126. https://doi.org/10.1016/j.wri.2020.100126.
[40] Mallapragada, S., Wadhwa, A., Agrawal, P., 2017. Antimicrobial peptides: The miraculous biological molecules. J Indian Soc Periodo 21, 434–438. https://doi.org/10.4103/jisp.jisp_325_16.
[41] Mauro, N., Schillaci, D., Varvarà, P., Cusimano, M.G., Geraci, D.M., Giuffrè, M., et al., 2018. Branched high molecular weight glycopolypeptide with broad-spectrum antimicrobial activity for the treatment of biofilm related infections. ACS Appl Mater Interfaces 10, 318–331. https://doi.org/10.1021/acsami.7b16573.
[42] Morshedy, A.S., Galhoum, A.A., Aleem, H.Abdel, Aleem, A., Shehab El-din, M.T., Okaba, D.M., et al., 2021. Functionalized aminophosphonate chitosan-magnetic nanocomposites for Cd(II) removal from aqueous solutions: performance and mechanisms of sorption. Appl Surf Sci 561, 150069. https://doi.org/10.1016/j.apsusc.2021.150069.
[43] Mucha, A., Kafarski, P., Berlicki, Ł., 2011. Remarkable potential of the α-aminophosphonate/phosphinate structural motif in medicinal chemistry. J Med Chem 54, 5955–5980. https://doi.org/10.1021/jm200587f.
[44] Neiber, R.R., Galhoum, A.A., El-Tantawy El Sayed, I., Guibal, E., Xin, J., Lu, X., 2022. Selective lead (II) sorption using aminophosphonate-based sorbents: effect of amine linker, characterization and sorption performance. Chem Eng J 442, 136300. https://doi.org/10.1016/j.cej.2022.136300.
[45] Ozkocaman, V., Ozcelik, T., Ali, R., Ozkalemkas, F., Ozkan, A., Ozakin, C., et al., 2006. *Bacillus spp*. among hospitalized patients with haematological malignancies: clinical features, epidemics and outcomes. J Hosp Infect 64, 169–176. https://doi.org/10.1016/j.jhin.2006.05.014.
[46] Paul, P., Chakraborty, P., Sarker, R.K., Chatterjee, A., Maiti, D., Das, A., et al., 2021. Tryptophan interferes with the quorum sensing and cell surface hydrophobicity of *Staphylococcus aureus*: a promising approach to inhibit the biofilm development. 3 Biotech 11, 376. https://doi.org/10.1007/s13205-021-02924-3.
[47] Qiu, J.-J., Xue, Q., Liu, Y.-Y., Pan, M., Liu, C.-M., 2014. A new polymer containing α-aminophosphonate unit used as reactive, halogen-free flame retardant for epoxy resins. Phosphorus, Sulfur, Silicon Relat Elem 189, 361–373. https://doi.org/10.1080/10426507.2013.819869.
[48] Rashad, M.M., El-Sayed, I.E., Galhoum, A.A., Abdeen, M.M., Mira, H.I., Elshehy, E. A., et al., 2021. Synthesis of α-aminophosphonate based sorbents – influence of inserted groups (carboxylic vs. amine) on uranyl sorption. Chem Eng J 421, 127830. https://doi.org/10.1016/j.cej.2020.127830.
[49] Rowe-Magnus, D.A., Kao, A.Y., Prieto, A.C., Pu, M., Kao, C., 2019. Cathelicidin peptides restrict bacterial growth via membrane perturbation and induction of reactive oxygen species. *American Soc Microbiol* 5, 10. https://doi.org/10.1128/mBio.02021-19.
[50] Saeed, S., Rashid, N., Ali, M., Hussain, R., 2010. Synthesis, characterization and antibacterial activity of nickel (II) and copper (II) complexes of N-(alkyl(aryl) carbamothioyl)-4-nitrobenzamide. Eur J Chem 1, 200–205. https://doi.org/10.5155/eurjchem.1.3.200-205.120.
[51] Samak, N.A., Selim, M.S., Hao, Z., Xing, J., 2022. Immobilized arginine/tryptophan-rich cyclic dodecapeptide on reduced graphene oxide anchored with manganese dioxide for microbial biofilm eradication. J Hazard Mater 426, 128035. https://doi.org/10.1016/j.jhazmat.2021.128035.
[52] Selim, M.S., Samak, N.A., Hao, Z., Xing, J., 2020. Facile design of reduced graphene oxide decorated with Cu_2O nanocube composite as antibiofilm active material. Mater Chem Phys 239, 122300. https://doi.org/10.1016/j.matchemphys.2019.122300.
[53] Shah, B., Chudasama, U., 2019. Kinetics, thermodynamics and metal separation studies of transition (Co^{2+}, Ni^{2+}, Cu^{2+}, Zn^{2+}) and heavy metal ions (Cd^{2+}, Hg^{2+}, Pb^{2+}) using novel hybrid ion exchanger: zirconium amino tris methylene phosphonic acid. Sep Sci Technol 54, 1560–1572. https://doi.org/10.1080/01496395.2018.1519580.
[54] Skok, Zi, Barančoková, M., Benek, Oe, Cruz, C.D., Tammela, Pi, Tomašič, T., et al., 2020. Exploring the chemical space of benzothiazole-based DNA gyrase B inhibitors. ACS Med Chem Lett 11, 2433–2440. https://doi.org/10.1021/acsmedchemlett.0c00416.
[55] Su, S., Chen, S., Fan, C., 2018. Recent advances in two-dimensional nanomaterials-based electrochemical sensors for environmental analysis. Green Energy Environ 3, 97–106. https://doi.org/10.1016/j.gee.2017.08.005.
[56] Takenaka, S., Iwaku, M., Hoshino, E., 2001. Artificial *Pseudomonas aeruginosa* biofilms and confocal laser scanning microscopic analysis. J Infect Chemother: J Jpn Soc Chemother 7, 87–93. https://doi.org/10.1007/s101560100014.
[57] USEPA, 2002. Health risks from microbial growth and biofilms in drinking water distribution systems, Washington, DC.
[58] Vaithyanathan, V.K., Cabana, H., Vaidyanathan, V.K., 2021. Remediation of trace organic contaminants from biosolids: influence of various pre-treatment strategies prior to *Bacillus subtilis* aerobic digestion. Chem Eng J 419, 129966. https://doi.org/10.1016/j.cej.2021.129966.
[59] van 't Hof, W., Veerman, E.C., Helmerhorst, E.J., Amerongen, A.V., 2001. Antimicrobial peptides: properties and applicability. Biol Chem 382, 597–619. https://doi.org/10.1515/BC.2001.072.
[60] Van Acker, H., Gielis, J., Acke, M., Cools, F., Cos, P., T C, 2016. The role of reactive oxygen species in antibiotic-induced cell death in *Burkholderia cepacia* complex bacteria. PLoS ONE 7 (11), 0159837. https://doi.org/10.1371/journal.pone.0159837.
[61] Vehapi, M., Özçimen, D., 2021. Antimicrobial and bacteriostatic activity of surfactants against *B. subtilis* for microbial cleaner formulation. Arch Microbiol 203, 3389–3397. https://doi.org/10.1007/s00203-021-02328-0.
[62] Vuong, C., Voyich, J.M., Fischer, E.R., Braughton, K.R., Whitney, A.R., DeLeo, F.R., et al., 2004. Polysaccharide intercellular adhesin (PIA) protects Staphylococcus epidermidis against major components of the human innate immune system. Cell Micro 6, 269–275. https://doi.org/10.1046/j.1462-5822.2004.00367.x.
[63] Wang, J., Ansari, M.F., Lin, J.-M., Zhou, C.-H., 2021. Design and synthesis of sulfanilamide aminophosphonates as novel antibacterial agents towards *Escherichia coli*. Chin J Chem 39, 2251–2263. https://doi.org/10.1002/cjoc.202100165.
[64] Wang, L., He, H., Zhang, C., Sun, L., Liu, S., Wang, S., 2016. Antimicrobial activity of silver loaded MnO_2 nanomaterials with different crystal phases against *Escherichia coli*. J Environ Sci 41, 112–120. https://doi.org/10.1016/j.jes.2015.04.026.
[65] Wang, Q., Zhu, M., Zhu, R., Lu, L., Yuan, C., Xing, S., et al., 2012. Exploration of α-aminophosphonate N-derivatives as novel, potent and selective inhibitors of protein tyrosine phosphatases. Eur J Med Chem 49, 354–364. https://doi.org/10.1016/j.ejmech.2012.01.038.
[66] Wilson, C., Lukowicz, R., Merchant, S., Valquier-Flynn, H., Caballero, J., Sandoval, J., et al., 2017. Quantitative and qualitative assessment methods for Biofilm growth: A mini-review. Res Rev J Eng Technol 6. ⟨https://www.rroij.com

/open-access/quantitative-and-qualitative-assessment-methods-for-biofilm-growth-a-minireview-.pdf).
[67] Xu, Y., Yan, K., Song, B., Xu, G., Yang, S., Xue, W., et al., 2006. Synthesis and antiviral bioactivities of α-aminophosphonates containing alkoxyethyl moieties. Molecules 11, 666–676. https://doi.org/10.3390/11090666.
[68] Zenobi, M.C., Luengo, C.V., Avena, M.J., Rueda, E.H., 2008. An ATR-FTIR study of different phosphonic acids in aqueous solution. Spectrochim Acta, Part A 70, 270–276. https://doi.org/10.1016/j.saa.2007.07.043.
[69] Zhang, C., Li, Y., Wang, C., Zheng, X., 2021. Different inactivation behaviors and mechanisms of representative pathogens (*Escherichia coli* bacteria, human adenoviruses and *Bacillus subtilis* spores) in g-C_3N_4-based metal-free visible-light-enabled photocatalytic disinfection. Sci Total Environ 755, 142588. https://doi.org/10.1016/j.scitotenv.2020.142588.